applied sciences

MDPI

Article

Universal Local Attractors on Graphs

Emmanouil Krasanakis *, Symeon Papadopoulos and Ioannis Kompatsiaris

Information Technologies Institute @ CERTH, 6th km Charilaou-Thermi, 57001 Thessaloniki, Greece; papadop@iti.gr (S.P.); ikom@iti.gr (I.K.)
* Correspondence: maniospas@iti.gr

Abstract: Being able to express broad families of equivariant or invariant attributed graph functions is a popular measuring stick of whether graph neural networks should be employed in practical applications. However, it is equally important to find deep local minima of losses (i.e., produce outputs with much smaller loss values compared to other minima), even when architectures cannot express global minima. In this work we introduce the architectural property of attracting optimization trajectories to local minima as a means of achieving smaller loss values. We take first steps in satisfying this property for losses defined over attributed undirected unweighted graphs with an architecture called *universal local attractor (ULA)*. This refines each dimension of end-to-end-trained node feature embeddings based on graph structure to track the optimization trajectories of losses satisfying some mild conditions. The refined dimensions are then linearly pooled to create predictions. We experiment on 11 tasks, from node classification to clique detection, on which ULA is comparable with or outperforms popular alternatives of similar or greater theoretical expressive power.

Keywords: graph neural networks; universal approximation; local attractors; diffusion; attributed graphs

Citation: Krasanakis, E.; Papadopoulos, S.; Kompatsiaris, I. Universal Local Attractors on Graphs. *Appl. Sci.* **2024**, *14*, 4533. https://doi.org/10.3390/app14114533

Academic Editors: Alessandro Rozza and Lorenzo Seidenari

Received: 18 April 2024
Revised: 17 May 2024
Accepted: 19 May 2024
Published: 25 May 2024

1. Introduction

Graph neural networks (GNNs) are a machine learning paradigm that processes graph-structured data by exchanging representations between linked nodes. Despite this paradigm's empirical success in tasks like node or graph classification, there are emerging concerns on its general applicability. Research has so far focused on the expressive power of GNNs, namely, their ability to tightly approximate attributed graph functions (AGFs). These take as input graphs whose nodes contain attribute vectors, such as features, embeddings, or positional encodings and create node or graph predictions (Section 2.3). Practically useful architectures, i.e., with a computationally tractable number of parameters that process finite graphs, have been shown to express certain families of AGFs, such as those that model WL-k tests (Section 2.3). In set theory terminology (Appendix A), the architectures are dense in the corresponding families.

Although satisfying WL-k or other tests is often taken as a gold standard of expressive power, it does not ensure that losses corresponding to training objectives are straightforward to minimize [1], or that the expressive power is enough to replicate arbitrary objectives. Therefore, applied GNNs should also easily find deep loss minima, in addition to any expressive power guarantees. In this work, the concept of deep minima refers to empirically achieving small loss values compared to other local minima. Although these values may not necessarily be close to the global minimum, they can still be considered better training outcomes compared to alternatives. We refer to minima that are not deep as shallow. These characterizations are informal, and demonstrated in Figure 1 for a real-valued loss function. Non-global minima in the figure are "bad local valleys" [2,3] in that they may trap optimization to suboptimal solutions. However, the premise of this work is that deep minima are acceptable given that they exhibit small-enough loss values.

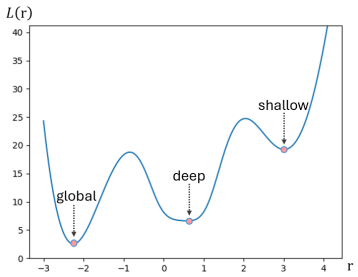

Figure 1. Different types of minima for a loss $\mathcal{L}(r)$ of one-dimensional prediction r of one sample.

In detail, we argue that the main challenge in deeply minimizing GNNs lies with the high-dimensional nature of loss landscapes defined over graphs, which exhibit many shallow valleys. (If we replaced GNNs with independent optimization for each node when only one graph was analyzed, we would not be able to impose structural properties that let the predictive performance generalize to validation and test data; this is demonstrated by experiment results for the MLP architecture in Section 5.) That is, there are many local minima with large loss values, corresponding to "bad" predictive ability, and optimization runs the risk of arriving near those and becoming trapped there. To understand this claim, Figure 2 presents the landscape of a loss defined on one triangle graph (i.e., three nodes linked pairwise). The third node makes optimization harder by creating many local minima of various depths when it obtains suboptimal values, for example, imposed by GNN architectures. We seek strategies that let deep minima attract optimization trajectories (as observed in the space of node predictions) while confining local minima attraction to small areas, for example, that initialization is unlikely to start from, or that the momentum terms of machine learning optimizers can escape from [4]. Theoretical justification of this hypothesis is left for future work, as here we probe whether architectures exhibiting local attraction properties can exist in the first place.

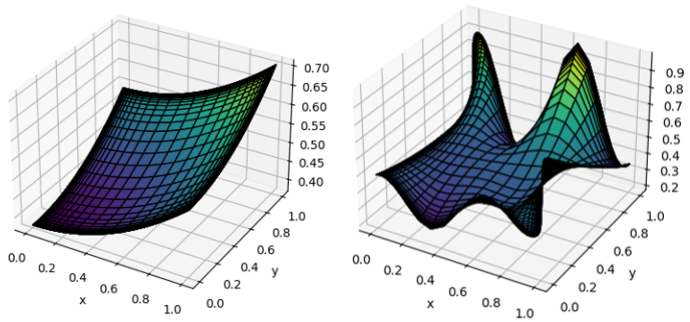

Figure 2. Landscape of a loss for values x, y, z of pairwise linked nodes produced for $x, y \in [0, 1]$ and ideal selection of z (**left**), and landscape of the same loss produced by a GNN architecture $[x, y, z]^T = \phi(\hat{M}[\theta_1, \theta_2, 0]^T)$ (**right**), where θ_1, θ_2 are trainable parameters and $[\cdot]^T$ are column vectors. For better visibility, lighter colors correspond to higher loss values..

Universally upholding local attraction is similar to universal approximation, barring two key differences: First, attraction is weaker in that it attempts to find local loss minima instead of tightly approximating functions (it approximates zero-loss gradients instead of zero loss). Second, the proposition is broader than many universal approximation results for practical architectures in that it is "universal" on more objectives (it is not restricted to tests like WL-k, even when the expressive power exhibits such restrictions). Here, we achieve local attraction with a novel GNN architecture called *universal local attractor (ULA)*. The mild conditions under which this architecture is universal can be found in Section 6.3. The process we follow to build it consists of three steps, which start from simple and progressively move to more complex settings:

Step 1. We analyze positive definite graph filters, which are graph signal processing constructs that diffuse node representations, like embeddings of node features, through links. Graph filters are already responsible for the homophilous propagation of predictions in predict-then-propagate GNNs (Section 2.2) and we examine their ability to track optimization trajectories of their posterior outputs when appropriate modifications are made to inputs. In this case, both inputs and outputs are one-dimensional.

Step 2. By injecting the prior modification process mentioned above in graph filtering pipelines, we end up creating a GNN architecture that can minimally edit input node representations to locally minimize loss functions given some mild conditions.

Step 3. We generalize our analysis to multidimensional node representations/features by folding the latter to one-dimensional counterparts while keeping track of which elements correspond to which dimension indexes, and transform inputs and outputs through linear relations to account for the different dimensions between them.

In experiments across 11 tasks, we explore the ability of ULA to learn deep minima by comparing it to several well-known GNNs of similar predictive power on example synthetic and real-world predictive tasks. In these, it remains consistently similar or better than the best-performing alternatives in terms of predictive performance, and always the best in terms of minimizing losses. Our contribution is threefold:

a. We introduce the concept of local attraction as a means of producing architectures whose training can reach deep local minima of many loss functions.
b. We develop ULA as a first example of an architecture that satisfies local attraction given the mild conditions summarized in Section 6.3.
c. We experimentally demonstrate the ability of ULA to find deep minima on training losses, as indicated by improvements compared to performant GNNs in new tasks.

This work is structured as follows. After this introductory section, Section 2 presents background on graph filters, graph neural networks, and related universal approximation terminology and results. Section 3 formalizes the local attraction property, and presents extensive theoretical analysis that incrementally constructs a first version of the ULA architecture that parses one-dimensional node features; we call this ULA1D. Section 4 generalizes ULA1D to multidimensional node features and outputs to obtain ULA, and describes the latter's theoretical properties and implementation needs. Section 5 presents experimental validation of our architecture's—and by extension the local attraction property's—practical usefulness. In particular, it finds similar or much deeper local minima than competitive alternatives across a collection of six synthetic and real-world settings. Section 6 discusses how ULA should be applied in practice, as well as threats to this work's validity. Finally, Section 7 summarizes our findings and presents prospective research directions.

2. Background

2.1. Graph Filters

Graph signal processing [5] extends traditional signal processing to graph-structured data by defining graph signals $h \in \mathbb{R}^{|\mathcal{V}|}$ that assign real values $h[v]$ to nodes $h \in \mathcal{V}$ (nodes and their integer identifiers are used interchangeably). It also considers node adjacency matrices M whose elements $M[u][v]$ hold either edge weights (1 for unweighted graphs) or zeros if the corresponding edges $u - v$ do not exist. Adjacency matrices are normalized as

$$\hat{M} = MD^{-1} \text{ or } \hat{M} = D^{-1/2}MD^{-1/2}$$

where D is the diagonal matrix of node degrees. Iterative matrix–vector multiplications $\hat{M}^n h$ express the propagation $n = 0, 1, 2, \ldots$ hops away from h. Throughout this work we adopt symmetrically normalized adjacency matrices of the second kind, as they are

also employed by graph convolutional networks (GCNs; see Section 2.2). A weighted aggregation of hops defines graph filters $F(\hat{M})$ and their posteriors r as

$$r = F(\hat{M})h \quad F(\hat{M}) = \sum_{n=0}^{\infty} f_n \hat{M}^n$$

for weights $\{f_n \in \mathbb{R} \,|\, n = 0, 1, 2, \dots\}$, indicating the importance placed on propagating graph signals n hops away. In this work, we focus on graph filters that are positive definite matrices, i.e., whose eigenvalues are all positive. We also assume a normalization $\sum_{n=0}^{\infty} f_n \leq 1$ for all filters, whose maximum eigenvalue then becomes

$$\lambda_{\max} = \max_{\lambda \in [-1,1]} F(\lambda) = \max_{\lambda \in [-1,1]} \sum_{n=0}^{\infty} f_n \lambda^n \leq \sum_{n=0}^{\infty} f_n \leq 1$$

where $\lambda \in [-1, 1]$ is the range of eigenvalues for symmetrically normalized adjacency matrices $\hat{M}$. Two well-known filters of this kind are personalized PageRank [6] and Heat Kernels [7]. These, respectively, arise from power degradation of hop weights $f_n = (1 - a)a^n$ and the exponential kernel $f_n = e^{-t}t^n/n!$ for parameters $a \in [0, 1]$ and $t \in \{1, 2, 3, \dots\}$.

2.2. Graph Neural Networks

Graph neural networks apply diffusion principles to multidimensional node features, for example, by defining layers that propagate nodes' features to neighbors one hop away, aggregating (e.g., averaging) them there, and transforming the result through linear neural layers with non-polynomial activations. To avoid oversmoothing that limits architectures to a couple of layers that do not to account for nodes many hops away, recursive schemes have been proposed to partially maintain early representations. Of these, our approach reuses the predict-then-propagate architecture, known as APPNP [8], which decouples the neural and graph diffusion components. It achieves this by first enlisting multilayer perceptrons to end-to-end train representations $H^{(L)} = MLP(H)$ of node features H by stacking linear layers ℓ endowed with $relu(x) = \{x \text{ if } x > 0, 0 \text{ otherwise}\}$ activation [9], and then, applying the personalized PageRank filter $ppr(\hat{M})$ on each representation dimension to arrive at final node predictions:

$$\begin{aligned} H^{(\ell)} &= \text{relu}(H^{(\ell-1)}W^{(\ell)} + b^{(\ell)}) \quad \ell = 1, 2, \dots, L \\ \hat{Y} &= \text{softmax}\big(ppr(\hat{M})H^{(L)}\big) \end{aligned} \tag{1}$$

A broader family of architectures that are often encountered as a concept throughout this work are message-passing GNNs (MPNNs) [10]. These aggregate representations from node neighborhoods, combine them with each node's own representation, and propagate them anew. Layers of this family can be written as

$$H^{(\ell)} = \phi^{(\ell)}\big(combine^{(\ell)}(H^{(\ell-1)}, aggregate^{(\ell)}(M, H^{(\ell-1)}))\big)$$

where the activation $\phi^{(\ell)}(\cdot)$ is the relu function in intermediate layers and, for classification tasks, becomes a softmax at the top representation layer. The $combine^{(\ell)}(\cdot, \cdot)$ mechanism is typically a row-wise concatenation followed by a linear layer transformation. It may also include element-by-element multiplication to be able to express the full class of WL-1 test, as for GNNML1 [11]. The aggregation step often accounts for some notion of the neighborhood around each node and can be as simple as an average across neighbors per $aggregate^{(\ell)}(M, H^{(\ell-1)}) = \widehat{M}H^{(\ell-1)}$ after adding self-loops to the graph [12] (adding self-loops is a common practice that is also employed by APPNP in Equation (1) to improve its diffusion component), or involve edge-wise attention based on the linked nodes [13].

For completeness, we present the mathematical formula of the graph convolutional network (GCN) architecture's layers:

$$H^{(\ell)} = \phi^{(\ell)}(\hat{M}H^{(\ell-1)}W^{(\ell)} + b^{(\ell)}) \tag{2}$$

where $W^{(\ell)}$ and $b^{(\ell)}$ are trainable weight matrices and bias vectors broadcast to all nodes.

2.3. Universal Approximation of AGFs

Typically, GNNs are required to be equivariant or invariant under node permutations. These properties correspond to outputs following the node permutations or being independent of them, respectively. An AGF $A(M, H)$ satisfies them if, for all attributed graphs (M, H) with adjacency matrices M and node features H,

$$A(\sigma M, \sigma H) = \sigma A(M, H) \qquad \text{(equivariance)}$$
$$A(\sigma M, \sigma H) = A(M, H) \qquad \text{(invariance)}$$

where σ is a matrix that permutes node order. We treat permutation as an operator. In this work, we tackle only equivariance, given that reduction mechanisms across nodes (e.g., an average of all feature values across nodes) turn equivariance into invariance. These properties are not inherently covered by the universal approximation theorems of traditional neural networks, which GNNs aim to generalize. It is, then, of interest to understand the expressive power of these architectures given that they satisfy one of the properties. In this way, one may obtain a sense of what to expect from their predictive ability.

Theoretical research has procured various universal approximation theorems for certain architectures that show either a general ability to approximate any AGF or the ability to differentiate graphs up to the Weisfeiler–Lehman isomorphism test of order k (WL-k), which is a weaker version of graph isomorphism. For example, WL-2 architectures can learn to at most recognize triangles but cannot necessarily differentiate between more complex structures, as shown in Figure 3. The folkore WL-k (FWL-k) test [14] has also been used as a non-overlapping alternative [15] (there is no clear distinction between the strengths of the two tests). Universal approximation is stronger than both in that it can perfectly detect isomorphism.

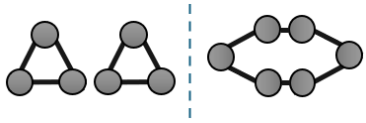

Figure 3. Two non-isomorphic graphs that can be distinguished by FWL-2 but not by WL-1 or WL-2.

Simple architectures, like GNNML1 [11], GCN [12], and APPNP [8], are at most as powerful as the WL-1 test in distinguishing between graphs of different structures, but remain popular for parsing large graphs thanks to their tractable implementations that take advantage of adjacency matrix sparsity to compute forward passes in times $O(|\mathcal{E}|\,L)$, where $|\mathcal{E}|$ is the number of graph edges and L the number of message-passing layers (usually 2, 5, 10, or 64 depending on the architecture and how well it tackles the oversmoothing problem). On the other hand, architectures like 1-2-3GNN [16] and PPGN [15] satisfy the WL-3 test but come at the cost of high computational demands (e.g., millions of hidden dimensions) by considering all tuples or triplets of node combinations, in the last case exhibiting computational complexity $\Theta(|\mathcal{V}|^3)$, where $|\mathcal{V}|$ is the number of nodes. For a summary on the expressive power of several architectures, refer to the work of Balcilar et al. [11], who also introduce the GNNML3 architecture to overcome these limits with appropriate injection of spectral node features.

In addition to WL-k or other types of limited expressiveness, some works tackle universal approximation over all AGFs. Historically, deep set learning [17] introduced universal approximation for equivariant and invariant functions over sets, and results

were quickly generalized to graph structures. However, such powerful architectures also suffer from computational intractability, like unbounded tensor order for internal representations [18], and the tensor order of internal representations needing to be at least half the number of input feature dimensions rounded down [19]. Increasing tensor order dimensions is so computationally intensive that these works experimented with graphs of few nodes.

An alternate research direction is to create MPNNs that, even though limited to WL-1 expressive power by themselves [16,20], can be strengthened with additional components. To this end, the generic message-passing scheme has been shown to be universal over Turing computable functions [1], although this does not cover the case of non-computable functions or density over certain sets of non-computable functions. More recent breakthroughs have shown that the expressive power is not necessarily a property of architectures alone, because enriching the node feature space with positional encodings [21,22], like random node representations, can make MPNNs more expressive [23]. A result that we use in later experiments is that MPNNs enriched with non-trainable node representations can express any non-attributed graph functions while retaining equivariance in probability [24].

For a comprehensive framework for working with node encodings, see the work of Keriven et al. [22]. In the latter, the authors criticize random node representations as non-perfectly equivariant, but in this work we adopt that methodology's motivating viewpoint that, in practice, equivariance in probability, by creating random values with the same process for each node, is nearly as good as hard-coded equivariance. At the very least, architectures endowed with random node representations can serve as a comparison with ULA.

2.4. Symbols

Table 1 summarizes symbols that we will be using throughout this work. In general, we use calligraphic letters to denote sets and parameterized functions, capital letters to denote matrices, and lowercase symbols to denote vectors or numeric values.

Table 1. List of symbols and their interpretation.

Symbol	Interpretation
$\mathcal{A}$	The set of all AGFs
$\mathcal{A}_\theta$	A GNN architecture function with parameters θ
$(M, H^{(0)})$	An attributed graph with adjacency M and features $H^{(0)}$
$\mathcal{A}_\theta(M, H)$	The node feature matrix predicted by $\mathcal{A}_\theta$ on attributed graph (M, H)
M	A graph adjacency matrix
$\mathcal{M}$	A finite or infinite set of attributed graphs
$\nabla_r \mathcal{L}(expr)$	Gradients of a loss computed at $r = expr$
$\hat{M}$	A normalized version of a graph adjacency matrix
$F(\hat{M})$	A graph filter of a normalized graph adjacency matrix; it is itself a matrix
X	A node feature matrix
Y	A node prediction matrix of a GNN
R	A node output matrix of ULA1D
H	A node representation matrix, often procured as a transformation of node features
$\mathcal{L}(A)$	A loss function $\mathcal{L} : \mathcal{A} \to [0, \infty)$ defined over AGFs A
$\mathcal{L}(M, X, Y)$	A loss function defined over attributed graphs (M, H) for node prediction matrix Y
$H^{(\ell)}$	Node representation matrix at layer ℓ of some architecture; nodes are rows
$W^{(\ell)}$	Learnable dense transformation weights at layer ℓ of a neural architecture
$b^{(\ell)}$	Learnable biases at layer ℓ of a neural architecture
$\phi^{(\ell)}$	Activation function at layer ℓ of a neural architecture
$cols(H^{(\ell)})$	The number of columns of matrix $H^{(\ell)}$
$ceil(x)$	The integer ceiling of real number x

Table 1. *Cont.*

Symbol	Interpretation
$\lvert \cdot \rvert$	The number of set elements
$\mathcal{V}$	The set of a graph's nodes
$\mathcal{E}$	The set of a graph's edges
$\mathcal{R}$	A domain in which some optimization takes place
θ_∞	Parameters leading to local optimum
Θ_{θ_∞}	A connected neighborhood of θ_∞
h_0	A graph signal prior from which optimization starts
r_∞	A locally optimal posterior graph signal of some loss
$\lVert \cdot \rVert$	The L2 norm
$\lVert \cdot \rVert_\infty$	The maximum element
$A\lvert B$	Horizontal matrix concatenation
$A;B$	Vertical matrix concatenation
MLP_θ	Multilayer perceptron with trainable parameters θ

3. One-Dimensional Local Attraction

In Section 3.1, we start by stating the generic form of the local attraction property. We then aim to satisfy that property with GNN architectures that employ positive definite graph filters as methods to diffuse information through edges. To this end, we conduct one-dimensional analysis with graph signals $h = H$ that are column vectors of dimension $|\mathcal{V}| \times 1$. These pass though positive definite graph filters to create posteriors $r = F(\hat{M})h$. In Section 3.2, we further constrain ourselves to optimization in one graph to create first local attraction properties for posteriors r. A first generalization of results that process graphs with an upper-bounded number of nodes is created in Section 3.3. These results directly generalize to multiple input and output dimensions in the next section.

The universal attractor that parses one-dimensional node representations H of any graph alongside other graph signals Dim required to minimize a loss is called ULA1D and presented in Figure 4. Broadly speaking, our goal is to learn new priors given all starting information—including original posteriors—that lead us to locally optimal posteriors $r = R = F(\hat{M})H^{(L)}$. This architecture can be trained end-to-end already to let R locally minimize losses. An intermediate component is a multilayer perceptron (MLP) that generates updated node representations to be diffused by graph filters. We generalize the architecture to multidimensional graph features with the methodology of Section 4, where features are unwrapped to vector form; jump forward to that section's introduction for an overview of the final ULA and where ULA1D fits in its forward pipeline.

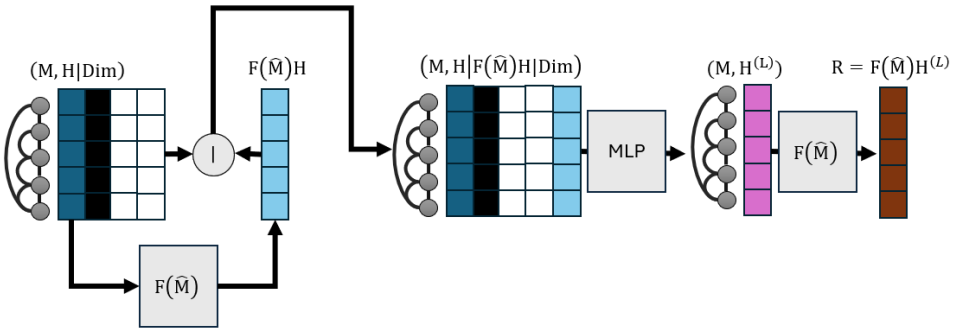

Figure 4. The one-dimensional universal local attractor (ULA1D) architecture; it obtains the outcome of diffusing the blue prior vector H through adjacency matrix M with a graph filter $F(\hat{M})$, and then, refines the posteriors. The refinement consists of concatenating the prior, the node information contributing to the loss function (black and white Dim), and the original posteriors to provide them as inputs to an MLP that learns new priors $H^{(L)}$. These in turn pass through the same graph filter to create new locally optimal posteriors R. Columns with the same colors represent the same data.

3.1. Problem Statement

Proposition 1 uses set theory terminology (Appendix A) to express our local attraction property, where $\|\cdot\|$ refers to the L2 norm. Our hypothesis is that this property is requisite for deeply optimizable GNNs. Intuitively, we seek architectures that, for any local minimum, admit a transformation of parameters that turns a connected neighborhood around the minimum into a loss plateau, i.e., an area with approximately near-zero gradient. We define loss plateaus with respect to gradients ∇_r of architecture outputs instead of parameter gradients ∇_θ. This avoids premature convergence that would "stall" due to architectural computations and not due to actual minimization of the loss. For example, we do not accept architectures that produce constant outputs when those are not local loss minima.

Proposition 1 (Locally attractive GNNs)**.** *Find architecture $\mathcal{A}_\theta$ with parameters $\theta \in \Theta$ in a connected compact set such that, for any parameters θ_∞ minimizing a differentiable loss $\mathcal{L}$ and any $\epsilon > 0$, there exists a parameter endomorphism S achieving $\|\nabla_r \mathcal{L}(\mathcal{A}_{S(\theta_0)})\| < \epsilon$ for any parameters θ_0 in some connected neighborhood of the minimum.*

If there exist multiple endomorphisms (i.e., transformations of parameters), one can select those that create plateaus which are more difficult to escape from when they encompass deep minima, but are easier to escape from when they contain only shallow local minima. For example, this can be achieved by controlling some of the attraction radii of Section 3.2. During this work's experimental validation, we select radii based on domain knowledge; our analysis reveals that the radii can be controlled by the diffusion rates of graph filters we employ, and thus, we look at the option of a personalized PageRank filter with a usually well-performing default diffusion parameter. Future research can make a more advanced search for appropriate filters that would create different radii.

Last, we tackle training objectives that can be expressed as a collection of sub-losses $\mathcal{L}(M, H, R)$ defined over a collection of attributed graphs $\mathcal{M} = \{(M, H)\}$, with node prior representations H and predicted node output representations R that we aim to discover. We can pool all losses to one quantity for a GNN architecture $\mathcal{A}_\theta$:

$$\mathcal{L}(\mathcal{A}_\theta) = \max_{(M,H)\in\mathcal{M}} \mathcal{L}(M, H, \mathcal{A}_\theta(M, H))$$

This setting can learn to approximate any equivariant AGF, and a reduction mechanism to node predictions can also learn invariant AGFs. However, the approximation is not dense (i.e., we cannot necessarily make it with arbitrarily small error, for example, because the architecture may not be expressive enough). The above setting also lets our analysis create functional approximations to non-functions, for example, that may include two conflicting loss terms for the same attributed graph. An implicit assumption of our analysis is that there exist architectural parameters that can replicate at least one local minimum.

3.2. Local Attractors for One-Dimensional Node Features in One Graph

To remain close to the original outputs of graph filters while also controlling for desired objectives, we adopt the practice of adjusting their inputs [25]. In this way, different outputs are at most as dissimilar as different inputs, given that by definition $\|F(\hat{M})h_0 - F(\hat{M})h\| \leq \lambda_{\max}\|h_0 - h\|$, where $\lambda_{\max} \leq 1$ is the filter's maximal eigenvalue when its parameters are normalized. As a first step, we exploit the structural robustness imposed by positive eigenvalues to create a local attraction area for some graph algorithm.

Consider starting priors $h_0 \in \mathbb{R}^{|\mathcal{V}|}$ and a twice-differentiable loss $\mathcal{L} : \mathcal{R} \to \mathbb{R}^{|\mathcal{V}|}$ on some compact domain $\mathcal{R} \subseteq \mathbb{R}^{|\mathcal{V}|}$ that has at least one local minimum (reminder: $|\mathcal{V}|$ is the number of nodes, and both priors and posteriors in our current setting are vectors that hold a numeric value for each node). Our goal is to find one such minimum while editing the priors. To this end, we argue that positive definite graph filters are so stable that they require only a rough approximation of the loss's gradients in the space of priors

to asymptotically converge to local optima for posteriors. This observation is codified in Theorem A1. We improve this result in Lemma A2, which sets up prior editing as the convergent point of a procedure that leads to posterior objective optimization without moving too far away from starting priors h_0.

Lemma 1. *For a positive definite graph filter $F(\hat{M})$ and differentiable loss $\mathcal{L}(r)$ over graph signal domain $\mathcal{R} \subseteq \mathbb{R}^{|\mathcal{V}|}$, update graph signals over time $t \in [0, \infty)$ per*

$$\begin{aligned} &\frac{\partial h(t)}{\partial t} = f(r(t)) \\ &r(t) = F(\hat{M})h(t) \\ &s.t.\ \|f(r) + \nabla_r \mathcal{L}(r)\| < \tfrac{\lambda_1}{\lambda_{\max}} \|\nabla_r \mathcal{L}(r)\| \text{ for all } \|\nabla_r \mathcal{L}(r)\| > 0, r \in \mathcal{R} \end{aligned}$$

where $\lambda_1, \lambda_{\max} > 0$ are the smallest positive and largest eigenvalues of $F(\hat{M})$, respectively. This leads to $\lim_{t\to\infty} \|\nabla_r \mathcal{L}(r(t))\| = 0$ if posteriors remain closed in the domain, i.e., if $r(t) \in \mathcal{R}$.

Proof. Essentially $f(r)$, which is the update rule for $h(t)$, roughly approximates the negative of the loss's gradients, similarly to gradient descent. Small inexactness in the approximation is absorbed by the positive definite filter's stability. A full mathematical proof is provided in Appendix B. □

Lemma 2. *Let a differentiable graph signal generation function $\mathcal{H}_\theta : \Theta \to \mathbb{R}^{|\mathcal{V}|}$ (the subscript θ is the function's H_θ input) on compact connected domain Θ admit some parameters $\theta_0 \in \Theta$ such that $\mathcal{H}_{\theta_0} = h_0$. If, for any parameters $\theta \in \Theta$, the Jacobian $\mathbb{J}_{\mathcal{H}_\theta}(\theta)$ has linearly independent rows (each row corresponds to a node) and satisfies*

$$\begin{aligned} &\left\|Err(\theta)\nabla_r \mathcal{L}(r)\right\| < \tfrac{\lambda_1}{\lambda_{\max}} \|\nabla_r \mathcal{L}(r)\| \quad \text{for all } \nabla \mathcal{L}(r) \neq \mathbf{0} \\ &Err(\theta) = \mathcal{I} - \mathbb{J}_{\mathcal{H}_\theta}(\theta)(\mathbb{J}^T_{\mathcal{H}_\theta}(\theta)\mathbb{J}_{\mathcal{H}_\theta}(\theta))^{-1}\mathbb{J}^T_{\mathcal{H}_\theta}(\theta) \\ &s.t.\ r(\theta) = F(\hat{M})\mathcal{H}_\theta \in \mathcal{H}_\Theta \end{aligned}$$

then there exist parameters $\theta_\infty \in \Theta$ such that $\|\nabla_r \mathcal{L}(r(\theta_\infty))\| = 0$.

Proof. The Jacobian $\mathbb{J}_{\mathcal{A}}(\theta)$ of θ is multiplied with the right pseudo-inverse of the difference, which will be close to the unit matrix for enough parameters. Empirically, $Err(\theta)$ is a matrix that represents differences between the pseudo-inverse multiplication and the unit matrix. Differences are then constrained to matter only for nodes with high-score gradient values. Thus, as long as the objective's gradient retains a clear—though maybe changing—direction to move towards, that direction can be captured by a prior generation model $\mathcal{A}_\theta$ of few parameters that may (or should) fail at following other kinds of trajectories. If such a model exists, there exists a parameter trajectory it can follow to arrive at locally optimal prior edits. A full mathematical proof is provided in Appendix B. □

We are now equipped with the necessary theoretical tools to show that neural networks are valid prior editing mechanisms as long as starting priors are close enough to ideal ones and some minimum architectural requirements are met. This constitutes a preliminary local attraction result that applies only to a graph signal processing pipeline and is codified in Theorem A1. A closed expression of the theorem's suggested architecture follows:

$$\begin{aligned} &\mathcal{A}_\theta(M, H) = F(\hat{M})H^{(L)} \\ &H^{(L)} = MLP_\theta(H^0) \\ &H^{(0)} = H|Dim|F(\hat{M})H \end{aligned} \tag{3}$$

where | is horizontal concatenation, the near-ideal priors are $\mathcal{A}_\theta(M, H) = R = r$, and MLP_θ represents the trainable multilayer perceptron that computes updated priors $H^{(L)}$ and parameters θ comprise all of its layer weights and biases. *Dim* represents any additional node information that determines the loss function's value.

Implementations should follow the data flow of Figure 4 presented at the beginning of this section. To show the existence of a neural network architecture, we use a specific universal approximation theorem that works well with our theoretical assumptions. However, other linear layers can replace the introduced one; at worst, and without loss of validity, these would be further approximations. The combination of an MLP component with propagation via graph filters sets up our architecture as a variant of the predict-then-propagate scheme after constructing an appropriate node feature matrix $H^{(0)}$.

Theorem 1. *Take the setting of Lemma A2, where the loss's Hessian matrix $\mathbb{H}_\mathcal{L}(r)$ linearly approximates the gradients $\nabla_r \mathcal{L}(r)$ within the domain $r \in \mathcal{R}$ with error at most $\epsilon_\mathbb{H}$. Let us construct a node feature matrix $H^{(0)}$ whose columns are graph signals (its rows $H^{(0)}[v]$ correspond to nodes v). If h_0, $F(\hat{M})h_0$, and all graph signals other than r involved in the calculation of $\mathcal{L}(r)$ are columns of $H^{(0)}$, and it holds that*

$$\frac{\lambda_1}{\lambda_{\max}} \|\nabla \mathcal{L}(r)\| > 2\epsilon_\mathbb{H} \|r - r_\infty\|$$

for any $r \in \mathcal{R} \setminus \{r_\infty\}$, then for any $\epsilon_\infty > 0$ there exists MLP_θ with relu activation, for which

$$\|F(\hat{M}) MLP_\theta(H^{(0)}) - r_\infty\| < \epsilon_\infty$$

Proof. Thanks to the universal approximation theorem (we use the form presented by [26] to work with non-compact domains and obtain sufficient layer widths), neural networks can produce tight-enough approximations of the desired trajectory gradients. At worst, there will be two layers to form a two-layer perceptron. We also use a second set of neural layers on top of the first to compute their integration outcome. A full mathematical proof is provided in Appendix B. □

Theorem A2 shows that any twice-differentiable loss can be optimized from points of a local area (this is a universal local attraction property), given that a sufficiently large L1 posterior regularization has been added to it. **Therefore the architecture of Theorem A1 is a local attractor of some unobserved base architecture, an unobserved feature transformation, and an unobserved parameter subdomain that nonetheless creates a known attraction radius in the space of posteriors.** Locally optimal posteriors cannot attract all optimization trajectories; the radius of the hypersphere domain from which ideal posteriors can always attract others is at worst $0.5|\mathcal{V}|\frac{\lambda_1}{\lambda_{\max}}$. Larger radii can be obtained for near-quadratic objectives, for which $\epsilon_\mathbb{H}$ is small. In practice, this can be imposed by also adding a large-enough L2 regularization, but we leave theoretical study of this option to future work.

If attraction hyperspheres are overlapping between local minima, it is uncertain which is selected. This is why we want to impose local attractiveness in the first place: to minimize overlaps between deep and shallow minima so that optimization can permanently escape from the attraction of the latter. Therefore, radii need to be large enough to enclose original posteriors within at least one hypersphere of nearby ideal ones, but not large enough to attract posteriors to shallow optima. For points farther away than the attraction radii from all local minima, it is unclear if any minimum would be found at all by a learning process.

A similar analysis to ours [27] points out that spectral graph theory research should move beyond low-pass filters and graphs with small eigenvalues. In this case, our worst attraction radius provides a rough intuition of which scenarios are easier to address. For example, we can explain why directly optimizing posteriors can lead to shallow optima [27]; direct optimization is equivalent to using the filter $F(\hat{M}) = I$, which exhibits a large optimization horizon radius $0.5|\mathcal{V}|$, and is, therefore, likely to enclose many local minima as

candidates towards which to adjust posteriors, including shallow ones. Conversely, filters that acknowledge the graph structure play the role of a minimum curation mechanism, which is a popular but previously unproven hypothesis [28,29] that we verify here.

Theorem 2. *There exists a sufficiently large parameter* $l_{reg} \in \left[0, 2\frac{\sup_h \|h-h_0\|}{|\mathcal{V}|}\right]$ *for which*

$$\tilde{\mathcal{L}}(r) = \mathcal{L}(r) + l_{reg}(\|r\|_1 - \|F(\hat{M})h_0\|_1)$$

satisfies the properties needed by Theorem A1 within the following domain:

$$\mathcal{R} = \{r_\infty\} \cup \left\{ r : \|r - r_\infty\| < 0.5 \max\left\{|\mathcal{V}|, \frac{\|\nabla\mathcal{L}(r)\|}{\epsilon_{\mathbb{H}}}\right\} \frac{\lambda_1}{\lambda_{\max}} \right\}$$

where r_∞ *is the ideal posteriors optimizing the regularized loss. If the second term of the* max *is selected, it suffices to have no regularization* $l_{reg} = 0$.

Proof. The area from which posteriors can be attracted to local optima is wider the closer to linear posterior objectives are. Furthermore, loss derivatives should also be large enough that when their norm is multiplied with Λ they still push optimization trajectories towards minima from faraway points of the domain. Large-enough L1 regularization translates to the l_{reg} derivative magnitude at each dimension. That is, it introduces a constant push of posteriors towards zero that keeps gradients sufficiently large. A full mathematical proof is provided in Appendix B. □

In the next subsection, we select losses with Lipschitz gradients. This means that Theorem A2 can create constrained attraction radii for $l_{reg} = 0$ given a graph filter with a small-enough eigenvalue ratio, as long as $\epsilon_H > 0$, which means that the loss should *not* be exactly the square distance from the starting posteriors. Although we select losses that also satisfy the Lipschitz gradient property throughout the rest of analysis, we keep the more general version of the theorem to support different future research directions too.

3.3. Attraction across Multiple Graphs

In Lemma A3 and Theorem A3, we now show that ULA1D (i.e., the architecture of Equation (3)) adheres to a universal minimization property over, respectively, finite and infinite collections of undirected unweighted attributed graphs with a bounded number of nodes. Both results can be applied for variants of the MLP component that use different universal approximation theorems, given that activation functions remain Lipschitz with Lipschitz gradients. The theorem stipulates some additional conditions that let us generalize the architecture's minimization to infinite sets of attributed graphs with one-dimensional node representations. We consider the conditions mild in that they are easy to satisfy. For example, node features may be (batch-)normalized to make them bounded.

Both theorems require a finite number of nodes of processed graphs to properly work with. This may be larger than the number of nodes in training graphs if similar substructures are encountered, but the theorems do not reveal an upper bound, and thus, the latter should be empirically evaluated in practical applications. At the same time, during the proof of Theorem A3 we employ a graph with a non-polynomial number of nodes that represents an equivalently hard problem. Theoretically, this means that our architecture could require a non-polynomial (though bounded) number of training data samples to learn under the required local attraction concerns. This only affects generalization power given the number of samples, i.e., whether low training and validation losses translate to low test losses, and is easy to check for in practice. Importantly, the space ULA1D implementations (and, by extension, the ULA implementation when we extend results to multidimensional node representations) is not only dense on local attractors but can actually reach them given enough training samples.

A final caveat of Theorem A3 is that for MLP activations that are not differentiable everywhere, the property of remaining in the local attraction area can theoretically be guaranteed only in probability. In particular, there may exist points (encountered with zero probability) with "infinite" derivatives that propel losses outside that area. In practice, though, activation functions are computed on finite machines where twice-differentiable relaxations can be considered in areas smaller than the numerical tolerance without affecting computational results. In this case, the dense subset of the neighborhood coincides with the full neighborhood. The theorem's version we present is geared towards future investigations of how limits in numerical tolerance could affect the local attraction property in practice.

Lemma 3. *Let a finite set of attributed graphs with undirected unweighted adjacency matrices M with up to a finite number of nodes v and one-dimensional node representations H be denoted as $\mathcal{M} = \{(M, H) : |\mathcal{V}| \leq v\}$. Let loss $\mathcal{L}(M, h, r)$ be twice-differentiable with respect to r and take any $\epsilon_\infty > 0$. Then, any selected θ_∞ that lets Equation (3) be a local loss minimum on all attributed graphs of $\mathcal{M}$ is contained in a connected neighborhood Θ_{θ_∞} of θ_∞ for which*

$$\|\nabla_r \mathcal{L}(M, H, \mathcal{A}_\theta(M, H))\| < \epsilon_\infty \text{ for any } (M, H) \in \mathcal{M} \text{ and } \theta \in \Theta_{\theta_\infty}$$

Proof. We generate a larger graph that comprises all subgraph structures and vertically concatenates corresponding node features. Thus, by reframing the small derivative outcome as an objective on this new attributed graph, Theorem A2 lets us minimize it to an arbitrarily small derivative. A full mathematical proof is provided in Appendix B. □

Theorem 3. *Consider infinite sets $\mathcal{M}$, bounded node feature values, Lipschitz loss gradients with respect to both h and r, and MLP_θ that has activation functions that are almost everywhere Lipschitz with Lipschitz derivatives (e.g., relu). Then, Lemma A3 holds for a dense subset of the neighborhood.*

Proof. Given that both the architecture and loss gradients are Lipschitz, similar pairs of node features will create similar gradients for the same adjacency matrices. We thus create a discretization of the domain of node features with small numerical tolerance. In this discretization, there is a finite number of possible adjacency matrices given the bounded number of graph nodes, and a finite number of values for each feature given that we discretize a bounded Euclidean space. Therefore, we have a finite (albeit non-polynomial) number of adjacency matrix and node feature combinations, and we can apply Lemma A3 to obtain small gradients, barring approximation errors that are related to the tolerance and can, thus, be controlled to also be small. The results hold for a dense subset of the neighborhood only to avoid points where activations are non-existing or non-Lipschitz derivatives. A full mathematical proof is provided in Appendix B. □

4. Universal Local Attractor

Previously, our analysis assumed one node feature and output dimension. We now create the ULA architecture, which generalizes the same analysis to any number of node feature and output dimensions. Our strategy for multidimensional universal attraction starts in Section 4.1 by considering settings where the number of node features and output dimensions are the same. In Section 4.2, we then add linear transformation layers to map actual node features X to lower-dimensional representations $H_{wrapped}$ (this helps reduce computational costs), and from optimized feature representations to architectural outputs Y with potentially different dimensions. A visualization of this scheme is presented in Figure 5, and in Section 4.3 we point to finer details that implementations should pay attention to. In Section 4.4, we finally discuss running time and memory complexity.

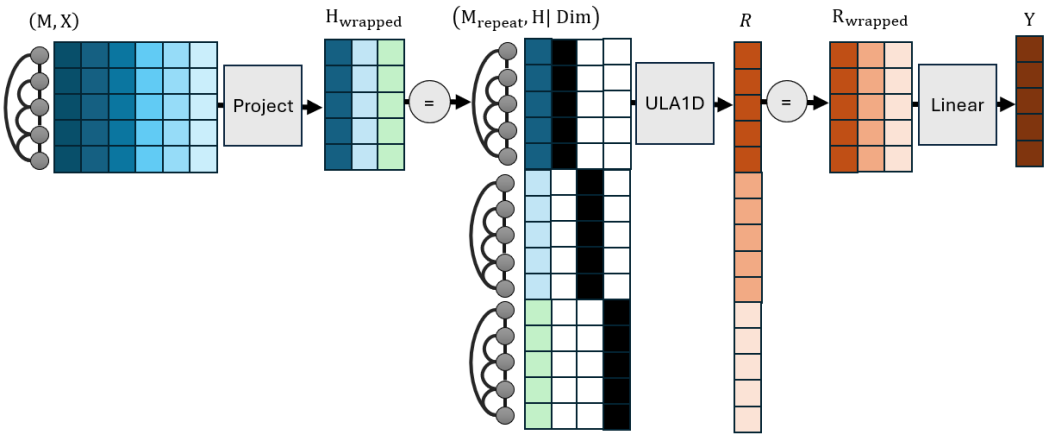

Figure 5. The ULA architecture pipeline based on its one-dimensional counterpart (ULA1D in Figure 4) that produces posteriors $H^{(L)}_{wrapped}$ given prior representations $H_{wrapped}$. The priors are unwrapped into a vector, and concatenated with an embedding of $H_{wrapped}$ feature dimension identifiers that each unwrapped row is retrieved from. Unwrapping also creates repetitions of the graph into a larger adjacency matrix M_{repeat} with M as its block diagonal elements. Outputs are rewrapped into matrix form. Linear layers change the dimensions of node features at the beginning and end of outputs at the end. Columns with the same colors represent the same data under the example projection. White and black columns represent example dimension encoding values.

4.1. Multidimensional Universal Attraction

First, we tackle the problem of multiple node feature dimensions to be diffused. Our strategy involves treating each node feature dimension as a separate graph signal defined on copies of the graph stacked together in a supergraph. We then optimize all dimensions by creating a supergraph of them. This also creates a signal that stacks all dimensions on top of each other. The methodology of this section is similar to the proof of Lemma A3 in that it vertically concatenates representations and creates an underlying supergraph. However, if we blindly performed an unwrapping of tensor H to a one-dimensional counterpart holding all its information, any computed loss function would not be symmetric with respect to the feature dimensions, as different dimensions require different outputs. This would mean that computations would not be invariant with respect to node features, as a permutation of features would create a different loss for different nodes.

To address this issue, we look back at Theorem A1, which stipulates that all necessary information to compute the loss should be included as columns of H. In our case, the necessary information consists of which feature dimension identifiers (i.e., the column numbers of H) each entry corresponds to. We can capture this either via a one-hot encoding or via an embedding representation; we opt for the second approach to avoid adding too many new dimensions to the one-dimensional unwrapped H; it suffices to learn $ceil(\log_2 K)$ or fewer embedding dimensions for $K = cols(H)$. Mathematically,

$$\begin{aligned}
&R = \mathcal{A}_\theta(M_{repeat}, H)\\
&H = (h_1; h_2; \ldots; h_K) \,|\, Dim\\
&Dim = \mathbf{1}Embed(1); \mathbf{1}Embed(2); \ldots; \mathbf{K}Embed(K)\\
&M_{repeat} = \begin{bmatrix} M & \mathbf{0} & \mathbf{0} & \ldots \\ \mathbf{0} & M & \mathbf{0} & \ldots \\ \mathbf{0} & \mathbf{0} & M & \ldots \\ \ldots & \ldots & \ldots & \ldots \end{bmatrix}\\
&\text{s.t. } H_{wrapped} = (h_1|h_2|\ldots|h_K)
\end{aligned} \tag{4}$$

where $\mathcal{A}_\theta$ is the ULA1D architecture, ; is vertical concatenation that vertically unwraps the representation matrix H, $|$ is horizontal concatenation, $\mathbf{0}$ is a matrix of zeroes of appropriate

dimension, $\mathbf{1}$ is a $|\mathcal{V}| \times 1$ matrix of ones, and *Embed* is a trainable embedding mechanism from integer identifiers to a $1 \times ceil(\log_2 K)$ matrix. To understand this formula, $\mathbf{1}Embed(1)$ are matrices that vertically repeat the corresponding embeddings $|\mathcal{V}|$ times to differentiate the feature dimension each row refers to. The concatenated result *Dim* has dimensions $(|\mathcal{V}|K) \times ceil(\log_2 K)$, where $|\mathcal{V}|K$ is the number of nodes in the new supergraph.

We now make use of ULA1D's theoretical properties to generate posteriors R that locally minimize the loss $\mathcal{L}(R) = \mathcal{L}(M_{repeat}, R)$ for every attributed graph (M_{repeat}, H). If the loss is equivariant, it is equivalent to defining an equivariant loss in terms of $(M, H_{wrapped})$ given a re-wrapping of R to matrix $R_{wrapped}$ with K columns:

$$\begin{aligned} &R_{wrapped} = (r_1|r_2|\ldots|r_K) \\ &\text{s.t. } R = (r_1; r_2 \ldots; r_K) \end{aligned} \tag{5}$$

for $|\mathcal{V}| \times 1$ vectors $r_1, r_2, \ldots, r_K$. We do not need additional theoretical analysis to show that any loss can be approximated, given that we reshaped how matrices are represented while leaving all computations the same and that, therefore, Theorems A1 and A2 still hold.

4.2. Different Node Feature and Prediction Dimensions

As a last step in designing our architecture, we introduce two additional layers as the first and last steps. In the former, we transform input features X to lower-dimensional representations $H_{wrapped}$ of dimension $K = col(H_{wrapped})$ that promote a computationally tractable architecture (Section 4.3). The output linear layer also maps from K representation dimensions to $col(Y)$ output dimensions.

Considering that R (and equivalently $R_{wrapped}$) is the outcome of the intermediate ULA1D that guarantees local attractiveness, the input and output transformation components are essentially part of the loss minimized by the ULA1D architecture of Equation (3). In particular, a loss function $\mathcal{L}_{multi}(M, X, Y)$ defined over ULA's multidimensional outputs Y is equivalent to minimizing the loss

$$\mathcal{L}(M, H, \mathcal{A}_\theta(H)) = \mathcal{L}_{multi}(M, Linear_X^{-1}(X), Linear_Y(\mathcal{A}_\theta(M, X)))$$

where $H = Linear_X(X)$, and $Linear_X$ and $Linear_Y$ are the input and output transformations, respectively. To enable an immediate application of local attractiveness results, the new loss needs to still have Lipschitz gradients, which in turn means that input and output transformations should *not* be able to approximate arbitrary functions, i.e., they cannot be MLPs. Furthermore, the input transformation needs to be invertible. Selecting both transformations as linear layers and setting $K \geq rank(H)$ satisfies both properties. For ease of implementation, we make transformation trainable, but they may also be extrapolated from informed ad hoc strategies, like node embeddings for matrix factorization.

4.3. Implementation Details

Implementations of the ULA architecture should take care to follow the following requisites for either theoretical analysis or common machine learning principles to apply. Ignoring any of these suggestions may cause ULA to become stuck in shallow local minima:

a. The output of ULA1D should be divided by 2 when the parameter initialization strategy of relu-activated layers is applied everywhere. This is needed to preserve input–output variance, given that there is an additional linear layer on top. This is not a hyperparameter. Contrary to the partial robustness to different variances exhibited by typical neural networks, having different variances between the input and output may mean that the original output starts from "bad" local minima, from which it may even fail to escape. In the implementation we experiment with later, failing to perform this division makes training become stuck near the architecture's initialization.
b. Dropout can only be applied before the output's linear transformation. We recognize that dropout is a necessary requirement for architectures to generalize well, but it can-

not be applied on input features due to the sparsity of the $H|Dim$ representation, and it cannot be applied on the $linear_X$ transformation due to breaking any (approximate) invertibility that is being learned.

c. Address the issue of dying neurons for ULA1D. Due to the few feature dimensions of this architecture, it is likely for all activations to become zero and make the architecture stop learning from certain samples from the beginning of training with randomly initialized parameters. In this work, we address this issue by employing a leaky relu $lrelu = \{x \text{ if } x \geq 0, 0.3x \text{ otherwise}\}$ as the activation function in place of $relu$. This change does not violate universal approximation results that we enlist. As per Theorem A3, activation functions should remain Lipschitz and have Lipschitz derivatives almost everywhere; both properties are satisfied by $prelu$.

d. Adopt a late stopping training strategy that repeats training epochs until both training and validation losses do not decrease for a number of epochs. This strategy lets training overcome saddle points where ULA creates a small derivative. For a more thorough discussion of this phenomenon refer to Section 6.2.

e. Retain linear input and output transformations, and do not apply feature dropout. We previously mentioned the necessity of the first stipulation, but the second is also needed to maintain Lipschitz loss derivatives for the internal ULA1D architecture.

4.4. Running Time and Memory

In Appendix C, we analyze the proposed architecture's running time and memory consumption in big-O complexity notation. These are

$$\begin{aligned} time &\in O\big(|\mathcal{E}|NK\log K + |\mathcal{V}|K(\log^2 K + col(X) + col(Y))\big) \\ memory &\in O(|\mathcal{E}| + |\mathcal{V}|K\log K + K(col(X) + col(Y))) \end{aligned}$$

where N is the number of the graph filter's parameters (we implement filters of finite diffusion breadth, for which $f_n = 0$ for $n > N$), and $K = col(H)$, the number of hidden node feature dimensions. Both time and memory complexity grow slightly worse than linearly as we choose more hidden dimensions, but our architecture remains computationally tractable in that it exhibits worse-than-linear scalability by a logarithmic scale of a well-controlled quantity. This is incomparable to the exponential increase in computations that would be incurred if GNNs satisfying universal approximation added more tensor dimensions.

Still, in terms of absolute orders of magnitude, the logarithmic scale inside the running time analysis is $\log_2 K$; for $K = 64$ selected in experiments, there is a 6-fold increase in running time and memory compared to simply running an APPNP architecture for graph diffusion. Factoring in that propagation through graph filter runs twice (once to obtain initial posteriors, and then, to refine them again), we obtain an approximate 12-fold increase in running time compared to APPNP. This means that large graphs residing at the limits of existing computing resources could be hard to process with ULA. Still, our architecture runs faster and consumes less memory than GCNII of those we compare with in Section 5.2.

In the experiments, we employ GPUs that let us parallelize feature dimensions, and hence, reduce the number of hidden dimension multiplications from $O(K)$ to $O(1)$ for the purposes of running time analysis. That is, the running time complexity under this parallelization is divided by K. Performant implementation of sparse matrix multiplication is not achievable by existing GPU frameworks, and for graphs with a small-enough number of nodes that can fit the adjacency matrix in GPU memory we prefer dense matrices and corresponding operations. In this case, instead of diffusion requiring $|\mathcal{E}|$ computations it should be substituted with $|\mathcal{V}|^2$ in the above complexities. We also adopt this to speed up experiments given that we train hundreds of architectures for hundreds of training epochs each, but in larger graphs the sparse computational model is both faster and more memory-efficient.

5. Experiments

In this section, we use ULA to approximate various AGFs and compare it against several popular architectures. In Appendix D, we show that ULA can be represented with an appropriate MPNN; it essentially adds constraints to which parameter combinations can be learned to satisfy the local attraction property. Consequently, our architecture's expressive power is at most WL-1 and we compare it with well-performing alternatives of at most as much expressive power, as described in Section 5.2. We also perform an investigative comparison against an MPNN enriched with random node representations for greater expressive power. The tasks we experiment on are described in Section 5.1 and span graph analysis algorithms and node classification. The experimentation code is based on PyTorch Geometric [30], and is available online as open source (https://github.com/MKLab-ITI/ugnn, accessed on 15 April 2024). We conduct all experiments on a machine with 16 GB RAM and 6 GB GPU memory.

5.1. Tasks

For our evaluation, we created a collection of synthetic and real-world tasks. Of these, the synthetic tasks present various degrees of expressive power and difficulty in being optimized by GNN architectures (including ULA). Each comprises a set of 500 synthetically generated graphs of uniformly chosen numbers of $[25, 100]$ nodes. There is a uniformly random $[0, 0.1]$ chance of linking each pair of nodes, with an added line path across all nodes in each graph to make them connected. The tasks we compute for these graphs are described below, where 4Clique and LongShort require more than WL-1 expressive power to be densely approximated. Class distributions for subgraph detection tasks are presented in Figure 6.

Degree. Learning to count the number of neighbors of each node. Nodes are provided with a one-hot encoding of their identifiers within the graph, which is a non-equivariant input that architectures need to learn to transfer to equivariant objectives. We do not experiment with variations (e.g., other types of node encodings) that are promising for the improvement of predictive efficacy, as this is a basic go-to strategy and our goal is not—in this work—to find the best architectures but instead assess local attractiveness. To simplify the experiment setup, we converted this discretized task into a classification one, where node degrees are the known classes.

Triangle. Learning to count the number of triangles. Similarly to before, nodes are provided with a one-hot encoding of their identifiers within the graph, and we convert this discretized task into a classification one, where the node degrees observed in the training set are the known classes.

4Clique. Learning to identify whether each node belongs to a clique of at least four members. Similarly to before, nodes are provided with a one-hot encoding of their identifiers within the graph. Detecting instead of counting cliques yields a comparable number of nodes between the positive and negative outcome, so as to avoid complicating assessment that would need to account for class imbalances. We further improve class balance with a uniformly random number of a $[0, 0.5]$ chance of linking nodes. Due to the high computational complexity of creating the training dataset, we restrict this task only to graphs with a uniformly random number of $[5, 20]$ nodes.

LongShort. Learning the length of the longest among the shortest paths from each node to all others. Similarly to before, nodes are provided with a one-hot encoding of their identifiers within the graph, and we convert this discretized task into a classification one, where path lengths in training data are the known classes.

Propagate. This task aims to relearn the classification of an APPNP architecture with randomly initialized weights and uniformly random $\alpha \in [0, 0.9]$ (the same for all graphs) that is applied on nodes with 16 feature dimensions, uniformly random features in the range $[0, 1]$, and four output classes. This task effectively assesses our ability to reproduce a graph algorithm. It is harder than the node classification settings below in that features are continuous.

0.9Propagate. This is the same as the previous task but with fixed $\alpha = 0.9$. Essentially, this is perfectly replicable by APPNP because the latter uses the same architecture with the same hyperparameters (α, layer dimensions, number of dense layers, number of propagation steps) and only needs to find the same randomly initialized layer weights. Hence, any failure of APPNP in finding deep minima for this task should be attributed to the need for better optimization strategies.
Diffuse. This is the same task as above, with the difference that the aim is to directly replicate output scores in the range $[0, 1]$ for each of the four output dimensions (these are not soft-maximized).
0.9Diffuse. This is the same as the previous task with fixed $\alpha = 0.9$. Similarly to 0.9Propagate, this task is in theory perfectly replicable by APPNP.

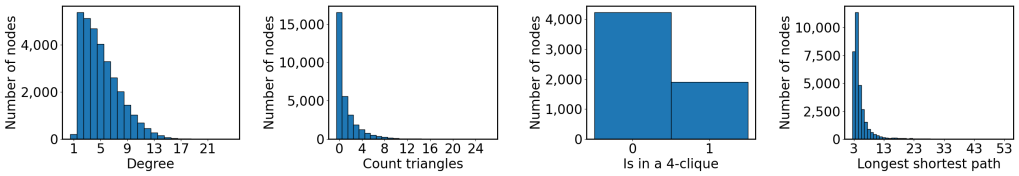

Figure 6. Distributions (in that order) of degrees, triangle counts, existence of 4-cliques, and longest shortest path distances in synthetic graphs.

In addition to the above, we also conduct node inference experiments across the following three real-world attributed graphs. These are used for the evaluation of GNNs for node classification, and we point out that they run on only one graph. In general, WL-1 architectures are accepted as the best-performing on these datasets, as there is no need to distinguish between different graphs:

Cora [31]. A graph that comprises 2708 nodes and 57,884 edges. Its nodes exhibit 3703 feature dimensions and are classified into one among seven classes.
Citeseer [32]. A graph that comprises 3327 nodes and 10,556 edges. Its nodes exhibit 1433 feature dimensions and are classified into one among six classes.
Pubmed [33]. A graph that comprises 19,717 nodes and 88,651 edges. Its nodes exhibit 500 feature dimensions and are classified into one among three classes.

5.2. Compared Architectures

We select architectures that are conceptually similar to ours in that they employ graph diffusion mechanisms. All architectures used for experiments are MPNNs, which means that they exhibit at most WL-1 expressive power. Therefore, we may safely attribute differences in predictive efficacy as the hardness of optimizing them.

MLP. A two-layer perceptron that does not leverage any graph information. We use this as a baseline to measure the success of graph learning.
GCN [12]. The architecture described by Equation (2). It comprises two linear layers, the first of which is followed by a *relu* activation.
GAT [13]. A gated attention network that learns to construct edge weights based on the representations at each edge's ends, and uses the weights to aggregate neighbor representations.
GCNII [34]. An attempt to create a deeper variant of GCN that is explicitly designed to be able to replicate the diffusion processes of graph filters if needed. We employ the variation with 64 layers.
APPNP [8]. The predict-then-propagate architecture with ppr base filter. Switching to different filters lets this approach maintain roughly similar performance, and we opt for its usage due to it being a standard player in GNN evaluation methodologies.
ULA [this work]. Our universal local attractor presented in this work. Motivated by the success of APPNP on node classification tasks, we also adopt the first 10 iterations of personalized PageRank as the filter of choice, and leave further improvements by tuning the filter to future work.

Additionally, we compare our approach with one of greater expressive power:

GCNNRI. This is the GCN-like MPNN introduced by Abboud et al. [24]; it employs random node representations to admit greater (universal approximation) expressive power and serves as a state-of-the-art baseline. We adopt its publicly available implementation, which first transforms features through two GCN layers of Equation (2) and concatenates them with a feature matrix of equal dimensions sampled anew in each forward pass. Afterwards, GCNNRI applies three more GCN layers and then another three-layered MLP. The original architecture max-pooled node-level predictions before the last MLP to create an invariant output (i.e., one prediction for each graph), but we do not perform this to accommodate our experiment settings by retaining equivariance, and therefore, create a separate prediction for each node. We employ the variation that replaces half of the node feature dimensions with random representations.

5.3. Evaluation Methodology

Training process. For synthetically generated datasets, we create a 50%–25%–25% train–validation–test split across graphs, of which the training and validation graphs are, respectively, used to train the architecture, and to avoid overtraining by selecting parameters with minimal validation loss. For real-world graphs, we create an evaluation split that avoids class imbalance in the training set, and for this reason we perform stratified sampling to obtain 50, 50 validation, and 100 test nodes. In all settings, training epochs repeat until neither training nor validation loss decrease for a patience of 100 consecutive epochs. We retain parameter values corresponding to the best validation loss. We allow decreases in training losses to reset the stopping patience in order to prevent architectures from becoming stuck in shallow minima, especially at the beginning of training. This increases the training time of architectures to requiring up to 6000 epochs in some settings, but in return tends to find much deeper minima when convergence is slower. A related discussion is presented in Section 6.2. For classification tasks, including counting tasks where the output is an integer, the loss function is categorical cross-entropy after applying softmax activation on each architecture's outputs. For regression tasks, the loss function is the mean absolute error.

Predictive performance. For all settings, we measure either accuracy (acc; larger is better) or mean absolute error (mabs; smaller is better) and compute their average across five experiment repetitions. We report these quantities instead of the loss because we aim to create practically useful architectures that can accurately approximate a wide range of AGF objectives. Evaluation that directly considers loss function values is even more favorable for our approach (see Section 6), though of limited practical usefulness. Since we are making a comparison between several architectures, we also compute Nemenyi ranks; for each experiment repetition, we rank architectures based on which is better (rank 1 is the best, rank 2 the second best, and so on) and average these across each task's repetition, and afterwards across all tasks. In the end, we employ the Friedman test to reject the null hypothesis that architectures are the same at the 0.05 p-value level, and then, check for statistically significant differences at the 0.05 p-value level between every architecture and ULA with the two-tailed Bonferroni–Dunn test [35], which Demsar [36] sets up as a stronger variant of the Nemenyi test [37]. For our results of $5 \times 11 = 55$ comparisons and seven compared methods, the test has critically difference $CD = 1.1$ rounded up; rank differences of this value or greater are considered statistically significant. We employ the Bonferroni–Dunn test because it is both strong and easy to intuitively understand.

Assessing minimization capabilities. To check whether we succeed in our main goal of finding deep minima, we also replicate experiments by equalizing training, validation, and test sets and investigating how well architectures can replicate the AGFs they are meant to reproduce. That is, we investigate the ability of architectures to either overtrain, as this is a key property of universal approximation or, failing that, to universally minimize objectives. Note that success in **this type of evaluation (i.e., success in overtraining) is**

the property we are mainly interested in this work, as it remains an open question for GNNs. The measured predictive performance mainly lets us see how well the learned AGFs generalize.

Hyperparameter selection. To maintain a fair comparison between the compared architectures, we employ the same hyperparameters for the same conceptually similar choices by repeating common defaults across the GNN literature. In particular, we use the same number of 64 output dimensions for each trained linear layer. We also use an 0.6 dropout rate for node features in all outputs of 64-layer representations except for ULA's input and output layers, which do not accept dropout. For GAT, we use the number of attention heads tuned on the Cora dataset, which is eight. All architectures are also trained using the Adam optimizer with learning rate 0.01 (this is the commonly accepted default for GNNs) and use default values for other parameters. For all other choices, like diffusion rates, we defer to architecture defaults. We initialize dense parameters with Kaiming initialization [38]. Due to already high computational demands, we did not perform extensive hyperparameter tuning, other than a simple verification that statistically significant changes could not be induced for both the Degree and Cora tasks (we selected these as conceptually simple) by modifying parameters or injecting or removing layers. In Section 6.4, we explain why this is not a substantial threat to the validity of the evaluation outcomes.

5.4. Experiment Results

Table 2 summarizes the experimental results across all tasks. In the case of generalization, ULA remains close to the best-performing architectures, which vary across experiments. This corroborates its universal minimization property, i.e., minimizing a wide breadth of objectives. There are certain tasks in which our approach is not the best, but this can be attributed to intrinsic shortcomings of cross-entropy as a loss function that at best approximates accuracy; even in cases where accuracy was not the highest, losses were smaller during experimentation (Section 6.1). Even better, the experimental results reveal that ULA successfully finds deep local minima, as indicated by its very ability to overtrain, something which other architectures are not always capable of.

A somewhat unexpected finding is that ULA outperforms GCNNRI in almost all experiments despite the significantly worse theoretical expressive power. We do not necessarily expect this outcome to persist across all real-world tasks and experiment repetitions, but it clearly indicates that (universal) local attraction may be a property more useful than universal approximation in certain situations. Overall, the Friedman test asserts that at least one approach is different than the rest, and differences between ULA and all other architectures are statistically significant by the Bonferroni–Dunn test when all tasks are considered, both when generalizing and when attempting to overtrain.

From a high-level point of view, we argue that there is no meaning to devising GNNs with rich expressive power without accompanying training strategies that can unlock that power. For example, ULA exhibiting imperfect but over 95% accuracy in overtrained node classification in the three real-world graphs could be an upper limit for our approach's expressive power, but it is a limit that is henceforth known to be achievable. Furthermore, overtrained ULA, and in some cases GCN and GCNNRI, outperform overtrained MLP on these tasks, where the latter essentially identifies nodes based on their features. This suggests that the graph structure can indeed help find deeper minima. Another example of expressive power not being the main limiting factor of predictive performance is that APPNP is always outperformed by ULA—and often by other architectures too—in the 0.9Diffusion and 0.9Propagation tasks, despite theoretically modeling them with exact precision (the two tasks use APPNP itself to generate node scores and labels, respectively).

Table 2. Evaluations of predictive performance and their Nemenyi ranks in parentheses across five repetitions of each task. For each task, best performance is in **bold**. Arrows indicate whether better measure values are larger (↑) or smaller (↓).

Task	Eval.	MLP	GCN [12]	APPNP [8]	GAT [13]	GCNII [34]	GCNNRI [24]	ULA
				Generalization				
Degree	acc ↑	0.162 (5.6)	0.293 (2.8)	0.160 (6.2)	0.166 (5.6)	0.174 (4.6)	0.473 (2.0)	**0.541** (1.2)
Triangle	acc ↑	0.522 (5.2)	0.523 (3.6)	0.522 (5.2)	0.522 (5.2)	0.522 (5.2)	0.554 (2.4)	**0.568** (1.2)
4Clique	acc ↑	0.678 (4.9)	0.708 (4.1)	0.677 (6.2)	0.678 (4.9)	0.678 (4.9)	0.846 (2.0)	**0.870** (1.0)
LongShort	acc ↑	0.347 (5.8)	0.399 (3.0)	0.344 (6.4)	0.350 (4.2)	0.348 (5.6)	0.597 (2.0)	**0.653** (1.0)
Diffuse	mabs ↓	0.035 (4.0)	0.032 (2.8)	0.067 (7.0)	0.035 (5.0)	0.037 (6.0)	0.030 (2.2)	**0.012** (1.0)
0.9Diffuse	mabs ↓	0.021 (4.6)	0.015 (3.0)	0.034 (7.0)	0.021 (4.4)	0.021 (6.0)	0.009 (1.8)	**0.007** (1.2)
Propagate	acc ↑	0.531 (2.6)	0.501 (4.0)	0.510 (3.6)	0.455 (6.1)	0.443 (6.9)	0.503 (3.8)	**0.861** (1.0)
0.9Propagate	acc ↑	0.436 (5.3)	0.503 (3.0)	0.452 (4.0)	0.418 (5.8)	0.401 (6.7)	0.546 (2.2)	**0.846** (1.0)
Cora	acc ↑	0.683 (6.6)	0.855 (4.2)	**0.866** (1.4)	0.850 (4.1)	0.863 (2.4)	0.696 (6.4)	0.859 (2.9)
Citeseer	acc ↑	0.594 (6.0)	0.663 (3.9)	0.676 (2.3)	0.661 (4.0)	**0.679** (1.8)	0.443 (7.0)	0.669 (3.0)
Pubmed	acc ↑	0.778 (6.4)	0.825 (3.7)	0.835 (2.0)	0.821 (4.0)	0.835 (2.1)	0.747 (6.6)	0.829 (3.2)
Average (CD = 1.1)		(5.2)	(3.5)	(4.7)	(4.8)	(4.7)	(3.5)	(1.6)
				Deepness (overtraining capability)				
Degree	acc ↑	0.172 (5.7)	0.331 (3.0)	0.170 (6.6)	0.175 (5.7)	0.186 (4.0)	**0.632** (1.2)	0.571 (1.8)
Triangle	acc ↑	0.510 (4.7)	0.510 (4.2)	0.510 (4.7)	0.510 (4.7)	0.510 (4.7)	0.536 (3.8)	**0.568** (1.2)
4Clique	acc ↑	0.665 (5.0)	0.779 (3.0)	0.657 (6.4)	0.665 (5.0)	0.663 (5.6)	**0.898** (1.4)	0.894 (1.6)
LongShort	acc ↑	0.347 (6.0)	0.391 (3.0)	0.347 (6.0)	0.351 (4.0)	0.347 (6.0)	0.588 (2.0)	**0.688** (1.0)
Diffuse	mabs ↓	0.032 (4.4)	0.028 (3.0)	0.061 (7.0)	0.032 (4.6)	0.033 (6.0)	0.026 (2.0)	**0.012** (1.0)
0.9Diffuse	mabs ↓	0.021 (4.6)	0.015 (3.0)	0.034 (7.0)	0.021 (4.4)	0.021 (6.0)	0.009 (1.8)	**0.007** (1.2)
Propagate	acc ↑	0.477 (4.2)	0.502 (2.4)	0.454 (4.4)	0.461 (4.9)	0.413 (6.6)	0.503 (4.5)	**0.844** (1.0)
0.9Propagate	acc ↑	0.493 (4.8)	0.527 (2.8)	0.534 (3.2)	0.444 (6.3)	0.451 (6.5)	0.534 (3.4)	**0.873** (1.0)
Cora	acc ↑	0.905 (5.6)	0.914 (3.2)	0.905 (5.4)	0.911 (3.8)	0.864 (7.0)	0.930 (2.0)	**0.996** (1.0)
Citeseer	acc ↑	0.865 (2.2)	0.818 (3.8)	0.794 (6.0)	0.808 (5.0)	0.767 (7.0)	0.849 (3.0)	**0.959** (1.0)
Pubmed	acc ↑	0.868 (3.8)	0.871 (2.0)	0.862 (5.2)	0.855 (6.8)	0.859 (6.0)	0.869 (3.2)	**0.956** (1.0)
Average (CD = 1.1)		(4.2)	(3.0)	(5.6)	(5.0)	(6.0)	(2.6)	(1.2)

6. Discussion

In this section, we discuss various aspects of ULA with respect to its practical viability. In Section 6.1, we observe that our architecture being occasionally outperformed by other methods when trying to generalize stems from the gap between accuracy and the categorical cross-entropy loss employed during training; ULA always finds deeper local optima for the latter. Then, in Section 6.2 we describe convergence speed and observe the existence of groking phenomena that are needed to escape from shallow local minima. Finally, in Section 6.3 we summarize the mild requirements needed for practical usage of ULA, and in Section 6.4 we point out threats to this work's validity.

6.1. Limitations of Cross-Entropy.

In the generalization portion of Table 2, ULA is not always the best-performing architecture. This happens because when minimization reaches minima of similarly low loss values other architectures incorporate implicit assumptions about the form of the final predictions that effectively regularize it to a favorable choice. For example, the smoothness constraint imposed by APPNP and GCNII layers often establishes them as the most accurate methods for the node classification datasets, which are known to be strongly homophilic (i.e., neighbors tend to have similar labels). This happens at the cost of the same assumptions drastically failing to induce deep minima in other tasks. Therefore, there is still merit in architectures curated for specific types of problems, as these may be enriched with hypotheses that let shallows losses generalize better. On the other hand, ULA should be preferred for solving unknown (black box) problems. Experimental validation is still required, because expressive power is also a limiting factor of our approach and hard

problems could require a lot of data and architecture parameters to train (Section 6.4 includes a more in-depth discussion of this concern).

Even when ULA is not the best approach, accuracy differences with the best approach are small and, importantly, we empirically verified that it still finds deeper minima for the optimized loss functions. For example, in Table 3 we show train, validation, and test losses and accuracies of all trained architectures in a Cora experiment at the point where best validation loss is achieved. We also show the minimum train loss achieved throughout all training, which occurs at a different point. In this case study, ULA indeed finds the deepest validation loss minimum, which means that the lesser predictive ability compared to alternatives comes both from (a) differences between validation and test losses, and (b) the discrepancy between minimizing categorical cross-entropy and finding maximal accuracy.

It is standard practice to employ categorical cross-entropy as a loss function in lieu of other accuracy maximization objectives, as a differentiable relaxation. However, based on our findings, following the same practice for node classification warrants further investigation, at least for inductive learning with a small number of samples. For example, adversarial variants of the loss function could help improve generalization to true accuracy when classification outcomes are not too certain. Finally, we verify that node features are expressive enough to find deep loss minima with MLP, but the graph structure is needed both to find deeper minima and to generalize to the validation and test splits.

Table 3. Differences between accuracy maximization and categorical cross-entropy minimization on one Cora experiment. The best value of each column is in **bold**.

	loss (↓)			**acc** (↑)		
	Train	Valid	Test	Train	Valid	Test
MLP	**0.113** (min 0.103)	1.061	1.059	**1.000**	0.657	0.659
GCN	0.198 (min 0.194)	0.541	0.564	0.986	0.863	**0.860**
APPNP	0.288 (min 0.284)	0.544	**0.563**	0.971	**0.869**	**0.860**
GAT	0.261 (min 0.254)	0.546	0.574	0.983	0.866	0.854
GCNII	0.425 (min 0.423)	0.656	0.668	0.951	0.866	0.849
GCNNRI	0.262 (min 0.015)	0.839	0.936	0.929	0.789	0.759
ULA	0.161 (min **0.007**)	**0.479**	0.890	0.974	0.854	0.846

6.2. Convergence Speed and Late Stopping

Universal attraction creates regions of small gradient values. However, some of these could form around saddle points through which optimization trajectories pass. These could also be shallow local minima that optimization strategies like Adam's momentum can overcome. To let learning strategies overcome such phenomena, in this work we train GNNs by employing a late stopping criterion. In this, we stop training only if neither training nor validation loss has decreased for a set number of epochs, called the patience. Early stopping at the point where validation losses no longer decrease with a patience of 100 epochs is already standard practice in the GNN literature. In this work, we employ late stopping with the same patience for all architectures to make a fair comparison; ULA needs it and we make a point to not underestimate the efficacy of the literature with early stopping.

Late stopping comes at the cost of additional computational demands, as training takes place over more (e.g., a couple of thousand instead of a couple of hundred) epochs. However, in Figure 7 we demonstrate that this practice could be necessary, at least for ULA, by investigating the progress of losses in a LongShort experiment, which is a "hard" AGF to learn given that it needs to consider the whole graph for each prediction. In this figure, there is a shallow loss plateau early on that spans hundreds of epochs and early stopping would have halted training prematurely.

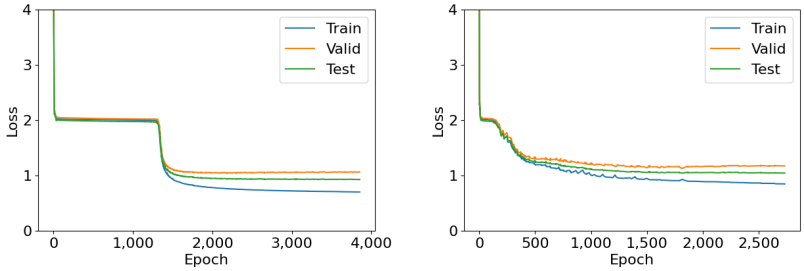

Figure 7. Convergence of train, validation, and test set losses of ULA (**left**) and GCNRNI (**right**).

6.3. Requirements to Apply ULA

Here, we summarize the conditions needed to employ ULA in new settings while benefiting from its local attraction property. We consider these mild, in that they are already satisfied by many settings. In addition to checking these conditions in new settings, make sure to follow the necessary implementation details of Section 4.3, as seen in our publicly available implementation at the experiment repository.

a. The first condition is that processed graphs should be unweighted and undirected. Normalizing adjacency matrices is accepted (we perform this in experiments—in fact it is necessary to obtain the spectral graph filters we work with), but structurally isomorphic graphs should obtain the same edge weights after normalization; otherwise, Theorem A3 cannot hold in its present form. Future theoretical analysis can consider discretizing edge weights to obtain more powerful results.
b. Furthermore, loss functions and output activations should be twice-differentiable, and each of their gradient dimensions should be Lipschitz. Our results can be easily extended to differentiable losses with continuous non-infinite gradients by framing their linearization needed by Theorem A1 as a locally Lipschitz derivative. However, more rigorous analysis is needed to extend results to non-differentiable losses, even when these are differentiable almost everywhere.
c. Lipschitz continuity of loss and activation derivatives is typically easy to satisfy, as any Lipschitz constant is acceptable. That said, higher constant values are expected to create architectures that are harder to train, as they require more fine-grained discretization to separate between graphs with similar attributes. Note that *the output activation is considered part of the loss* in our analysis, which can drastically simplify matters. Characteristically, passing softmax activation through a categorical cross-entropy loss is known to create gradients equal to the difference between predictions and true labels, which is a 1-Lipschitz function, and therefore, accepts ULA. Furthermore, having no activation with mabs or L2 loss is admissible in regression strategies, as this loss has a 1-Lipschitz derivative. However, employing higher powers of score differences or KL-divergence is not acceptable, as their second derivatives are unbounded, and thus, their first derivatives are not Lipschitz.
d. Finally, ULA admits powerful minimization strategies but requires positional encodings to exhibit stronger expressive power. To this end, we suggest following progress in the respective literature.

6.4. Threats to Validity

Before closing this work, we point to threats to validity that future research based on this work should account for. To begin with, we introduced local attraction as a property that induces deep loss minima thanks to allowing training losses to escape from shallow local minima. This is a claim that we did not verify through analysis. The results discussed above, like ULA's efficacy in finding smaller loss values in all cases and the groking behavior align with our hypothesis. However, it also requires theoretical justification that we left for future work. For example, investigation is needed on how valleys or local maxima are

affected by the plateaus we forcefully create. Despite the current lack of such theoretical results, we reiterate the importance of this work as a first demonstration that GNNs with the local attraction property actually exist and could be useful.

In terms of experimental validation, we did not perform hyperparameter tuning due to the broad range of experiment settings we visited. This is a threat to interpreting exact assessment values of the provided architectures, as improved alternatives could exist. However, our main point of interest was to understand substantial qualitative differences between architectures that cannot be bridged by hyperparameter tuning. For example, ULA exhibits close to double the predictive accuracy compared to the similarly powerful GCN in some tasks of Table 2. For existing architectures, we also verified that adding or removing one representation transformation layer, selecting representation dimensions between $\{32, 64, 128\}$ and selecting learning rates between $\{0.1, 0.01, 0.001\}$ did not improve predictive efficacy for the Degree and Cora settings by any noticeable amount, but a more principled exploration can be conducted by benchmarking papers.

Choosing paper defaults could err in favor of overestimating the abilities of existing GNNs on the non-synthetic graphs, in that we select only architectures and parameters that are both tuned and known to work well. We employ this practice because it does not raise concerns over our approach's viability, and given that otherwise computationally intensive experimentation would be needed to tune hyperparameters in all settings.

Finally, the evaluation considers a number of 100 synthetic graphs with up to 500 nodes, again mainly due to computational constraints of larger-scale experimentation. This number of graphs was empirically selected as sufficient for small predictive differences between training and validation sets across all experiments. For graphs with more nodes, ULA could require a non-polynomial number of hidden layer dimensions, as revealed by the intermediate step in our proofs. Thus, for harder tasks and without sufficient training data or number of parameters, other architectures could reach deeper minima. Furthermore, we can never extrapolate efficacy to an unbounded number of nodes, because theoretical results do not hold in that scenario. Instead, graphs with the maximum number of nodes that will be seen in practice should be included in validation sets. Finally, if an insufficient number of training samples is provided, overtraining—even with validation precautions—persists as a risk to be assessed, especially for an approach tailored to deep minimization.

7. Conclusions and Future Directions

In this work, we introduced the local minimization property as a means of creating GNN architectures that can find deep minima of loss functions, even when they cannot express the best fit. We then created the ULA architecture that refines the predict-then-propagate scheme to become a local attractor for a wide range of losses. We experimentally corroborated that this architecture can find deep local minima in a collection of several tasks compared to others of similar or greater expressive power. Thus, local attraction and, in general, properties that improve the deepness of learned minima deserve closer scrutiny; they are especially useful when assumptions about the predictive task (e.g., whether it can be best supported by homophilous diffusion) cannot be made a priori, in which case universally promising options are sought out.

Future works need to properly analyze the benefits of local attraction beyond the empirical understanding gleaned from our experiments. In particular, our results can be combined with optimization theory and loss landscape analysis of traditional neural networks [3]. Furthermore, local attractors with controlled attraction areas could serve as alternatives to GNN architecture search [39], and ULA could be combined with architectures exhibiting greater expressive power, especially FPGNN [15], which exhibits WL-3 while also applying MLPs on all node feature dimensions. Moreover, concerns over a potentially large breadth or width of intermediate layers can be met by devising mechanisms that create (coarse) invariant representations of each graph's structure. Finally, compatibility or trade-offs between universal AGF approximation and local attractiveness should be investigated.

Author Contributions: Conceptualization, E.K. and S.P.; data curation, E.K.; formal analysis, E.K.; funding acquisition, S.P. and I.K.; investigation, E.K.; methodology, E.K.; project administration, S.P. and I.K.; resources, S.P. and I.K.; software, E.K.; supervision, S.P.; validation, E.K., S.P., and I.K.; visualization, E.K.; writing—original draft, E.K.; writing—review and editing, Symeon Papadopoulos. All authors have read and agreed to the published version of the manuscript.

Funding: This work and the APC were partially funded by the European Commission under contract number H2020-951911 AI4Media, and by the European Union under the Horizon Europe MAMMOth project, Grant Agreement ID: 101070285. UK participant in Horizon Europe Project MAMMOth is supported by UKRI grant number 10041914 (Trilateral Research LTD).

Institutional Review Board Statement: Not applicable.

Informed Consent Statement: Not applicable.

Data Availability Statement: Experiments, datasets, and implemented architectures can be found online at https://github.com/MKLab-ITI/ugnn, accessed on 15 April 2024.

Conflicts of Interest: The authors declare no conflicts of interest.

Appendix A. Terminology

For the sake of completeness, in this appendix we briefly describe several properties that we mention in the course of this work.

Boundedness. This is a property of quantities that admit a fixed upper numerical bound, matrices whose elements are bounded, or functions that output bounded values.

Closure. Closed sets are those that include all their limiting points. For example, a real-valued closed set that contains open intervals (a, b) also includes their limit points a, b.

Compactness. We use the sequential definition of compactness, for which compact sets are closed and bounded.

Connectivity. This is a property of sets that cannot be divided into two disjoint non-empty open subsets. Equivalently, all continuous functions from connected sets to $\{0, 1\}$ are constant.

Density. In the text we often claim that a space A is dense in a set B. The spaces often contain functions, in which case we consider a metric the worst deviation under any input, which sets up density as the universal approximation property of being able to find members of A that lie arbitrarily close to any desired elements of B.

Lipschitz continuity. We refer to multivariate multi-value functions $f(x)$ as c-Lipschitz if they satisfy the property $\|f(x_1) - f(x_2)\|_p \leq c\|x_1 - x_2\|_p$ for some chosen p-norm $\|\cdot\|_p$. Throughout this work, we consider this property for the norm $\|\cdot\|_\infty$, which computes the maximum of absolute values. If a Lipschitz function is differentiable, then it is c-Lipschitz only if $\|\nabla_x f(x)\| \leq c$. If two functions are Lipschitz, their composition and sum are also Lipschitz. If they are additionally bounded, their product is also Lipschitz.

Appendix B. Theoretical Proofs

Lemma A1. *For a positive definite graph filter $F(\hat{M})$ and differentiable loss $\mathcal{L}(r)$ over graph signal domain $\mathcal{R} \subseteq \mathbb{R}^{|\mathcal{V}|}$, update graph signals over time $t \in [0, \infty)$ as per*

$$\begin{aligned}
&\frac{\partial h(t)}{\partial t} = f(r(t)) \\
&r(t) = F(\hat{M})h(t) \\
&\text{s.t. } \|f(r) + \nabla_r \mathcal{L}(r)\| < \tfrac{\lambda_1}{\lambda_{\max}}\|\nabla_r \mathcal{L}(r)\| \text{ for all } \|\nabla_r \mathcal{L}(r)\| > 0, r \in \mathcal{R}
\end{aligned}$$

where $\lambda_1, \lambda_{\max} > 0$ are the smallest positive and largest eigenvalues of $F(\hat{M})$, respectively. This leads to $\lim_{t\to\infty} \|\nabla_r \mathcal{L}(r(t))\| = 0$ if posteriors remain closed in the domain, i.e., if $r(t) \in \mathcal{R}$.

Proof. For non-negative posteriors $r = F(\hat{M})h(t)$, and non-zero loss gradients, the Cauchy–Schwartz inequality in the bilinear space $\langle x, y\rangle = x^T F(\hat{M})y$ determined by the positive definite graph filter $F(\hat{M})$ yields

$$\begin{aligned}
\frac{d\mathcal{L}\big(r(t)\big)}{dt} &= \Big(\nabla_r \mathcal{L}\big(r(t)\big)\Big)^T F(\hat{M})\frac{dh(t)}{dt} = \Big(\nabla_r \mathcal{L}\big(r(t)\big)\Big)^T F(\hat{M}) f\big(r(t)\big) \\
&= \Big(\nabla_r \mathcal{L}\big(r(t)\big)\Big)^T F(\hat{M})\big(-\nabla_r \mathcal{L}\big(r(t)\big) + \big(f\big(r(t)\big) + \nabla_r \mathcal{L}\big(r(t)\big)\big)\big) \\
&\leq -\Big(\nabla_r \mathcal{L}\big(r(t)\big)\Big)^T F(\hat{M})\nabla_r \mathcal{L}\big(r(t)\big) + \big(\nabla_r \mathcal{L}(r)\big)^T F(\hat{M})\Big(f\big(r(t)\big) + \nabla_r \mathcal{L}\big(r(t)\big)\Big) \\
&\leq -\lambda_1 \|\nabla_r \mathcal{L}\big(r(t)\big)\|^2 + \lambda_{\max}\big\|f\big(r(t)\big) + \nabla \mathcal{L}\big(r(t)\big)\big\|\big\|\nabla \mathcal{L}\big(r(t)\big)\big\| \\
&< -\lambda_1 \big\|\nabla_r \mathcal{L}\big(r(t)\big)\big\|^2 + \lambda_{\max}\tfrac{\lambda_1}{\lambda_{\max}}\big\|\nabla_r \mathcal{L}\big(r(t)\big)\big\|\big\|\nabla \mathcal{L}\big(r(t)\big)\big\| \\
&= 0
\end{aligned}$$

where ^{T} is the matrix transposition symbol. Therefore, the loss asymptotically converges to a locally minimum point. □

Lemma A2. *Let a differentiable graph signal generation function $\mathcal{H}_\theta : \Theta \to \mathbb{R}^{|\mathcal{V}|}$ on compact connected domain Θ admit some parameters $\theta_0 \in \Theta$ such that $\mathcal{H}_{\theta_0} = h_0$. If, for any parameters $\theta \in \Theta$, the Jacobian $\mathbb{J}_{\mathcal{H}_\theta}(\theta)$ has linearly independent rows (each row corresponds to a node) and satisfies*

$$\begin{aligned}
&\big\|Err(\theta)\nabla_r \mathcal{L}(r)\big\| < \tfrac{\lambda_1}{\lambda_{\max}}\|\nabla_r \mathcal{L}(r)\| \quad \textit{for all } \nabla \mathcal{L}(r) \neq \boldsymbol{0} \\
&Err(\theta) = \mathcal{I} - \mathbb{J}_{\mathcal{H}_\theta}(\theta)(\mathbb{J}^T_{\mathcal{H}_\theta}(\theta)\mathbb{J}_{\mathcal{H}_\theta}(\theta))^{-1}\mathbb{J}^T_{\mathcal{H}_\theta}(\theta) \\
&\textit{s.t. } r(\theta) = F(\hat{M})\mathcal{H}_\theta \in \mathcal{H}_\Theta
\end{aligned}$$

then there exist parameters $\theta_\infty \in \Theta$ such that $\|\nabla_r \mathcal{L}\big(r(\theta_\infty)\big)\| = 0$.

Proof. Let us consider a differentiable trajectory for parameters $\theta(t)$ for times $t \in [0, \infty)$ that starts from $\theta(0) = \theta_0$ and (asymptotically) arrives at some $\theta_\infty = \lim_{t\to\infty}\theta(t)$. For this trajectory, it holds that $\frac{d\mathcal{H}_{\theta(t)}}{dt} = \mathbb{J}_{\mathcal{H}_\theta}\big(\theta(t)\big)\frac{d\theta(t)}{dt}$. Let us also consider the posteriors

$$r(t) = r(\theta(t)) = F(\hat{M})\mathcal{H}_{\theta(t)}$$

arising from the graph signal generation function $\mathcal{H}_{\theta(t)}$ at times t for parameters $\theta(t)$, as well as the least squares problem of minimizing the projection of the loss's gradient to the row space of $\mathbb{J}_{\mathcal{H}_\theta}\big(\theta(t)\big)$:

$$\text{minimize } \big\|\nabla_r \mathcal{L}\big(r(t)\big) - \mathbb{J}_{\mathcal{H}_\theta}\big(\theta(t)\big)x(t)\big\|$$

The closed form solution to this problem can be found by

$$x(t) = \big(\mathbb{J}_{\mathcal{H}_\theta}{}^T\big(\theta(t)\big)\mathbb{J}_{\mathcal{H}_\theta}\big(\theta(t)\big)\big)^{-1}\mathbb{J}^T_{\mathcal{H}_\theta}\big(\theta(t)\big)\nabla_\theta \mathcal{L}\big(r(t)\big)$$

Thus, as long as $h(t) = \mathcal{H}_{\theta(t)}$ (we will call this Proposition P.I), this lemma's first precondition can be written for posteriors $r(t) = F(\hat{M})h(t)$ and $\nabla_r \mathcal{L}\big(r(t)\big) \neq \mathbf{0}$ as

$$\big\|\nabla_r \mathcal{L}\big(r(t)\big) - \mathbb{J}_{\mathcal{H}_\theta}\big(\theta(t)\big)x(t)\big\| < \tfrac{\lambda_1}{\lambda_{\max}}\|\nabla_r \mathcal{L}\big(r(t)\big)\|$$

We now set $x(t)$ as the derivatives of some parameters across their trajectory, that is,

$$x(t) = \tfrac{d\theta(t)}{dt} \Rightarrow \Big\|\nabla_r \mathcal{L}\big(r(t)\big) - \tfrac{d\mathcal{H}_{\theta(t)}}{dt}\Big\| < \tfrac{\lambda_1}{\lambda_{\max}}\|\nabla_r \mathcal{L}\big(r(t)\big)\|$$

Therefore, from Lemma A1 we obtain that our system asymptotically arrives at locally optimal posteriors, i.e., with $\nabla_r \mathcal{L}(r_\infty) = 0$ for $r_\infty = \lim_{t\to\infty} r(t)$.

As a final step, we now investigate the priors signal editing converges at. For this, we can see that the update rule leads to the selection of priors $h(t)$ at times t for which

$$\frac{dh(t)}{dt} = \frac{d\mathcal{H}_{\theta(t)}}{dt} \Rightarrow \lim_{t\to\infty} h(t) = h(0) + \int_{t=0}^{\infty} \frac{\mathcal{H}_{\theta(t)}}{dt} dt = h(0) + \mathcal{H}_{\theta_\infty} - \mathcal{H}_{\theta_0} = \mathcal{H}_{\theta_\infty}$$

For some parameters $\theta_\infty = \lim_{t\to\infty} \theta(t)$. We can similarly show that Proposition P.I holds true. Hence, there exists an optimization path of prior editing parameters (not necessarily the same as the one followed by the optimization algorithm used in practice) that arrives at the edited priors $\mathcal{H}_{\theta_\infty}$ that let posteriors exhibit local optimality. □

Theorem A1. *Take the setting of Lemma A2, where the loss's Hessian matrix $\mathbb{H}_\mathcal{L}(r)$ linearly approximates the gradients $\nabla_r \mathcal{L}(r)$ within the domain $r \in \mathcal{R}$ with error at most $\epsilon_\mathbb{H}$. Let us construct a node feature matrix $H^{(0)}$ whose columns are graph signals (its rows $H^{(0)}[v]$ correspond to nodes v). If h_0, $F(\hat{M})h_0$, and all graph signals other than r involved in the calculation of $\mathcal{L}(r)$ are columns of $H^{(0)}$, and it holds that*

$$\frac{\lambda_1}{\lambda_{\max}} \|\nabla \mathcal{L}(r)\| > 2\epsilon_\mathbb{H} \|r - r_\infty\|$$

for any $r \in \mathcal{R} \setminus \{r_\infty\}$, then for any $\epsilon_\infty > 0$ there exists MLP_θ with relu activation, for which

$$\|F(\hat{M}) MLP_\theta(H^{(0)}) - r_\infty\| < \epsilon_\infty$$

Proof. Let $\mathbb{H}_\mathcal{L}(r)$ be the Hessian matrix of $\mathcal{L}(r)$ with respect to node values of the graph signal $r \in \mathcal{R}$ of a domain $\mathcal{R}$. Given that its rank is $K(r)$, there exists a decomposition $\mathbb{H}_\mathcal{L}(r) = J(r)D(r)$ with fixed inner dimensions $K_{\max} = \sup_{r\in\mathcal{R}} K(r)$. That is, $J(r)$ has dimensions $|\mathcal{V}| \times K_{\max}$ and $D(r)$ has dimensions $K_{\max} \times dim(\Theta)$, where $dim(\Theta)$ counts the dimensions of the parameter space Θ (i.e., is the number of parameters). When $K(r) = K_{\max}$, the decomposition even becomes unique for the particular r.

We now select a prior generation model $\mathcal{H}_\theta$ with linearly independent rows and a Jacobian $\mathbb{J}_{\mathcal{H}_\theta}(\theta)$ that is a function (e.g., an MLP) approximating well the first of the decomposition elements. That is, for any chosen small-enough *but non-negligible* constant $\epsilon_\mathbb{J} > 0$ within the domain $\mathcal{R}$ it holds that

$$\left\|\mathbb{J}_{\mathcal{H}_\theta}(\theta) - J(r)\right\| \leq \epsilon_\mathbb{J}$$

Throughout this proof, r is a function of θ, but we do not write $r(\theta)$ for simplicity. The Jacobian does not need to have linearly independent rows; small perturbations (with the cumulative effect that when added to the actual approximation error make it smaller than $\epsilon_\mathbb{J}$) can be injected in each row to make the rows of its approximation linearly independent. Additionally, we use the Hessian as a linear estimator of gradients $\nabla_r \mathcal{L}(r_\infty)$ as per

$$\|\nabla_r \mathcal{L}(r_\infty) - \nabla_r \mathcal{L}(r) - \mathbb{H}_\mathcal{L}(r)(r_\infty - r)\| \leq \epsilon_\mathbb{H} \|r - r_\infty\|$$

We now rewrite the loss's gradient as a linear transformation of a factor $\mathcal{L}'(r)$ with an error term $\epsilon(r)$:

$$\nabla_r \mathcal{L}(r) = \mathbb{J}_{\mathcal{H}_\theta}(\theta)\mathcal{L}'(r) + \epsilon(r)$$

where the factor is $\mathcal{L}'(r) = \mathbb{J}^T_{\mathcal{H}_\theta}(\theta)\left(\mathbb{J}_{\mathcal{M}_\theta}(\theta)\mathbb{J}^T_{\mathcal{M}_\theta}(\theta)\right)^{-1}\nabla\mathcal{L}(r_\infty) + D(r)(r - r_\infty)$, and the error term admits a small bound:

$$\|\epsilon(r)\| \leq \epsilon_\mathbb{H}\|r - r_\infty\| + \epsilon_\mathbb{J}\|D(r)\|\|r - r_\infty\| \leq \sup_{r\in\mathcal{R}} \|r - r_\infty\|(\epsilon_\mathbb{H} + \sup_{r\in\mathcal{R}} \|D(r)\|\epsilon_\mathbb{J})$$

At this point, we choose $\epsilon_\mathbb{J} = \frac{\epsilon_\mathbb{H}}{\sup_{r\in\mathcal{R}} \|D(r)\|}$, which yields $\|\epsilon(r)\| \leq 2\epsilon_\mathbb{H}\|r - r_\infty\|$.

Applying the linear estimation obtained above on the quantities of Lemma A2, we obtain

$$\begin{aligned}\left\|Err(\theta)\nabla_r\mathcal{L}(r)\right\| &= \|\nabla_r\mathcal{L}(r) - \mathbb{J}_{\mathcal{H}_\theta}(\theta)(\mathbb{J}^T_{\mathcal{H}_\theta}(\theta)\mathbb{J}_{\mathcal{H}_\theta}(\theta))^{-1}\mathbb{J}^T_{\mathcal{H}_\theta}(\theta)\left(\mathbb{J}_{\mathcal{H}_\theta}(\theta)\mathcal{L}'(r) + \epsilon(r)\right)\| \\ &= \|\nabla_r\mathcal{L}(r) - \mathbb{J}_{\mathcal{H}_\theta}(\theta)\mathcal{L}'(r) + \mathbb{J}_{\mathcal{H}_\theta}(\theta)(\mathbb{J}^T_{\mathcal{H}_\theta}(\theta)\mathbb{J}_{\mathcal{H}_\theta}(\theta))^{-1}\mathbb{J}^T_{\mathcal{H}_\theta}(\theta)\epsilon(r)\| \\ &= \|\epsilon(r) - \mathbb{J}_{\mathcal{H}_\theta}(\theta)(\mathbb{J}^T_{\mathcal{H}_\theta}(\theta)\mathbb{J}_{\mathcal{H}_\theta}(\theta))^{-1}\mathbb{J}^T_{\mathcal{H}_\theta}(\theta)\epsilon(r)\| = \left\|Err(\theta)\epsilon(r)\right\|\end{aligned}$$

However, the matrix $\mathcal{I} - Err(\theta) = \mathbb{J}_{\mathcal{H}_\theta}(\theta)(\mathbb{J}^T_{\mathcal{H}_\theta}(\theta)\mathbb{J}_{\mathcal{H}_\theta}(\theta))^{-1}\mathbb{J}^T_{\mathcal{H}_\theta}$ is idempotent (that is, it holds $(\mathcal{I} - Err(\theta))(\mathcal{I} - E) = \mathcal{I} - Err(\theta)$), and therefore, its eigenvalues are either 0 or 1. Thus,

$$\left\|Err(\theta)\nabla_r\mathcal{L}(r)\right\| \leq \|\epsilon(r)\| \leq 2\epsilon_{\mathbb{H}}\|r - r_\infty\| < \tfrac{\lambda_1}{\lambda_{\max}}\|\nabla_r\mathcal{L}(r)\|$$

Given that we showed the existence of a (deep neural network) function, $\mathbb{J}_{\mathcal{H}_\theta}(\theta)$, we integrate it to retrieve $\mathcal{H}_\theta$, and then, approximate the integral with a new deep neural network. Given the universal approximation theorem's form described by [26], the latter can be the architecture described by this theorem, used to produce error less than $\epsilon_\infty\frac{\lambda_1}{\lambda_{\max}}$. In this case,

$$\|F(\hat{A})H^{(L)} - r_\infty\| = \|F(\hat{A})H^{(L)} - F(\hat{A})\mathcal{H}_{\theta_\infty}\| \leq \|F(\hat{A})\|\|H^{(L)} - \mathcal{H}_{\theta_\infty}\| < \|\epsilon_\infty\|$$

We could not immediately assume the existence of that final network, because we needed to verify the Jacobian's properties for the function it approximates and "hide" methods of tracking equal partial derivatives of different nodes behind the term $\epsilon_{\mathbb{J}}$.

As a final remark, one of the preconditions for Lemma A2's application is for posteriors r to remain within the domain $\mathcal{R}$ enclosing $r_0 = F(\hat{M})h_0$. Effectively, this stipulates that r_0 is implicitly injected into the loss function as a choice on which direction to follow. One way to achieve this is demonstrated in Theorem A2. □

Theorem A2. *There exists a sufficiently large parameter* $l_{reg} \in \left[0, 2\frac{\sup_h\|h-h_0\|}{|\mathcal{V}|}\right]$ *for which*

$$\tilde{\mathcal{L}}(r) = \mathcal{L}(r) + l_{reg}(\|r\|_1 - \|F(\hat{M}h_0)\|_1)$$

satisfies the properties needed by Theorem A1 within the following domain:

$$\mathcal{R} = \{r_\infty\} \cup \left\{r : \|r - r_\infty\| < 0.5\max\left\{|\mathcal{V}|, \tfrac{\|\nabla\mathcal{L}(r)\|}{\epsilon_{\mathbb{H}}}\right\}\tfrac{\lambda_1}{\lambda_{\max}}\right\}$$

where r_∞ *is the ideal posteriors optimizing the regularized loss. If the second term of the* max *is selected, it suffices to have no regularization* $l_{reg} = 0$.

Proof. For ease of notation, during this proof we define $w = 0.5\frac{\lambda_1}{\lambda_{\max}}$. Without loss of generality, consider $sgn(\cdot)$ to be a twice-differentiable closure of the sign function on the optimization trajectory, i.e., a tight-enough approximation of the element-by-element sign operator. If $\tilde{\epsilon}_{\mathbb{H}}$ and $\epsilon_{\mathbb{H}}$ are the maximum derivative approximation errors of $\tilde{\mathcal{L}}(r)$ and $\mathcal{L}(r)$, respectively, it suffices to select $l_{reg} > 0$ such that

$$\begin{aligned}&w\|\nabla\mathcal{L}(r)\| + wl_{reg}|\mathcal{V}| > (\epsilon_{\mathbb{H}} + l_{reg})\sup_r\|r - r_\infty\| \\ &\Leftrightarrow l_{reg}(w|\mathcal{V}| - \sup_r\|r - r_\infty\|) > \epsilon_{\mathbb{H}}\sup_r\|r - r_\infty\| - w\|\nabla\mathcal{L}(r)\| \\ &\Leftarrow |\mathcal{V}|w > \sup_r\|r - r_\infty\| \text{ or } \epsilon_{\mathbb{H}}\sup_r\|r - r_\infty\| < w\|\nabla\mathcal{L}(r)\|\end{aligned}$$

where the first case needs to come alongside the condition

$$l_{reg} > \tfrac{\sup_r\|r-r_\infty\|}{w|\mathcal{V}|-\sup_r\|r-r_\infty\|} \Leftarrow l_{reg} \Leftarrow l_{reg} = \tfrac{\sup_r\|r-r_\infty\|}{w|\mathcal{V}|} \geq \tfrac{2w\|q-q_0\|}{w|\mathcal{V}|}$$

but in the second case it suffices to select any $l_{reg} \geq 0$. Given an appropriate selection, we obtain the necessary criterion:

$$w\|\tilde{\mathcal{L}}(r)\| \geq w\|\nabla\mathcal{L}(r)\| + wl_{reg}|\mathcal{V}| > (\epsilon_{\mathbb{H}} + l_{reg}) \sup_r \|r - r_\infty\| \geq \tilde{\epsilon}_{\mathcal{H}}\|r - r_\infty\|$$

□

Lemma A3. *Let a finite set of attributed graphs with undirected unweighted adjacency matrices M, with up to a finite number of nodes v and one-dimensional node representations H, be denoted as $\mathcal{M} = \{(M, H) : |\mathcal{V}| \leq v\}$. Let loss $\mathcal{L}(M, h, r)$ be twice-differentiable with respect to r and any $\epsilon_\infty > 0$. Then, any selected θ_∞ that lets Equation (3) be a local loss minimum on all attributed graphs of $\mathcal{M}$ is contained in a connected neighborhood Θ_{θ_∞} of θ_∞ for which*

$$\|\nabla_r\mathcal{L}(M, \mathcal{A}_\theta(M, H))\| < \epsilon_\infty \text{ for any } (M, H) \in \mathcal{M} \text{ and } \theta \in \Theta_{\theta_\infty}$$

Proof. Let us write $\mathcal{M} = \{(M_1, H_1), (M_2, H_2), (M_3, H_3) \dots\}$ and create the block-diagonal matrix

$$M = \begin{bmatrix} M_1 & \mathbf{0} & \mathbf{0} & \dots \\ \mathbf{0} & M_2 & \mathbf{0} & \dots \\ \mathbf{0} & \mathbf{0} & M_3 & \dots \\ \dots & \dots & \dots & \dots \end{bmatrix}$$

and the feature matrix $H = [H_1; H_2, H_3; \dots]$, where ; is the vertical concatenation symbol (do not forget that this lemma refers to the one-dimensional setting where $H_1, H_2, H_3, \dots$ are vectors, and therefore, H is also a vector.

By Theorem A2, the ULA1D architecture of Equation (3) admits parameters $\theta \in \Theta_{\theta_\infty}$ that reproduce gradient norm up to ϵ_∞ for any twice-differentiable loss, including the loss $\mathcal{L}_{all}(r)$ such that

$$\mathcal{L}_{all}(\mathcal{A}_\theta(M, H)) = \mathcal{L}(M_1, H_1, \mathcal{A}_\theta(M_1, H_1)) + \mathcal{L}(M_2, H_2, \mathcal{A}_\theta(M_2, H_2)) + \dots$$

It also holds that

$$F(\hat{M}) = \begin{bmatrix} F(\hat{M}_1) & \mathbf{0} & \mathbf{0} & \dots \\ \mathbf{0} & F(\hat{M}_2) & \mathbf{0} & \dots \\ \mathbf{0} & \mathbf{0} & F(\hat{M}_3) & \dots \\ \dots & \dots & \dots & \dots \end{bmatrix}$$

given that adjacency normalization considers only row and column degrees for each node, and potentially adding self-loops that add the unit matrix on the diagonal. Given this result, we now concatenate vertically all parts of our predictive pipeline to obtain that $\mathcal{A}_\theta(M, H) = [\mathcal{A}_\theta(M_1, H_1); \mathcal{A}_\theta(M_2, H_2); \mathcal{A}_\theta(M_3, H_3); \dots]$. Thus, for any element i of $\mathcal{M}$, we obtain

$$\|\nabla_r\mathcal{L}(M_i, H_i, \mathcal{A}_\theta(M_i, H_i))\| \leq \|\nabla_r\mathcal{L}_{all}(r)\| \leq \epsilon_\infty$$

As a final remark, we stress that previous theoretical results were obtained for a finite number of nodes, and for this reason this proof only works on a set $\mathcal{M}$ with a finite number of elements, which set up M as the adjacency matrix of a graph with a finite number of nodes (the sum of all nodes in the set of graphs). Handling an infinite number of graphs is tackled in the proof of Theorem A3 that follows. □

Theorem A3. *Consider infinite sets $\mathcal{M}$, bounded node feature values, Lipschitz loss gradients with respect to both h and r, and MLP_θ that has activation functions that are almost everywhere Lipschitz with Lipschitz derivatives (e.g., relu). Then, Lemma A3 holds for a dense subset of the neighborhood.*

Proof. Our chosen $\mathcal{A}_\theta(M, H)$ is $c(\theta)$-Lipschitz with respect to H for some value $c(\theta) > 0$, as it is composed from Lipschitz functions (activations and linear matrix multiplications and additions). Consider that $\mathcal{L}$ has a $c_\mathcal{L}$-Lipschitz derivative. We can now write

$$\|\mathcal{A}_\theta(M, H_i) - \mathcal{A}_\theta(M, H_j)\|_\infty \leq c(\theta)\|H_i - H_j\|_\infty$$
$$\Rightarrow \|\nabla_r \mathcal{L}(M, H_i, \mathcal{A}_\theta(M, H_i)) - \nabla_r \mathcal{L}(M, H_i, \mathcal{A}_\theta(M, H_j))\|_\infty \leq c_\mathcal{L} c(\theta)\|H_i - H_j\|_\infty$$

where $\|\cdot\|_\infty$ obtains the maximum absolute value of vector elements. Similarly, the quantity

$$errdif(\theta) = \nabla_r \mathcal{L}(M, H_i, \mathcal{A}_\theta(M, H_i)) - \nabla_r \mathcal{L}(M, H_i, \mathcal{A}_\theta(M, H_j))$$

is c_{ge}-Lipschitz with respect to θ for some constant $c_{ge} > 0$, i.e., $\|errdif(\theta_i) - errdiff(\theta_j)\| \leq c_{ge}\|\theta_i - \theta_j\|_\infty$. Note that above all loses have H_i as the second argument. We also have that the quantity

$$apprfeats(H_i) = \nabla_r \mathcal{L}(M, H_i, \mathcal{A}_\theta(M, H_j))$$

is c_{fe}-Lipschitz with respect to H_i for some constant $c_{fe} > 0$, i.e.,
$\|apprfeats(H_i) - apprfeats(H_j)\| \leq c_{fe}\|H_i - H_j\|_\infty$.

At the same time, consider the discretization of the feature space H that creates a collection for numerical precision $\epsilon_{prec} > 0$, whose exact value will be selected later on:

$$\mathcal{M}_{\epsilon_{prec}} = \{(M, ceil(\tfrac{H}{\epsilon_{prec}} - 0.5)\epsilon_{prec}) : (M, H) \in \mathcal{M}\}$$

For the discretization it holds that, for every $(M, H) \in \mathcal{M}$ and θ there exists the closest element in $(M, H') \in \mathcal{M}_{\epsilon_{prec}}$, for which

$$H' = \arg \min_{(M,H') \in \mathcal{M}_{c(\theta)}} \|H - H'\|_\infty \leq \epsilon_{prec}$$
$$\Rightarrow \|\nabla_r \mathcal{L}(M, H, A_\theta(M, H)) - \nabla_r \mathcal{L}(M, H, A_\theta(M, H'))\|$$
$$\leq c_\mathcal{L} c(\theta)\|H - H'\| \leq c_\mathcal{L} c(\theta)\epsilon_{prec}\frac{\sqrt{|\mathcal{V}|}}{2}$$

Having established bounds for the error of replacing elements of $\mathcal{M}$ with their discretized equivalents, we now move on to the main proof. Consider any $\epsilon_\infty > 0$, select a fixed ϵ_{prec} with appropriate value (we will see how to determine this later). Now, the discretization has a number of elements upper-bounded by a finite number:

$$|\mathcal{M}_{\epsilon_{prec}}| \leq 2^{|\mathcal{V}|(|\mathcal{V}|+1)/2} ceil\left(\tfrac{diff}{\epsilon_{prec}}\right)^{col(H)}$$

where $diff = \sup_{H_i, H_j} \|H_i - H_j\|_\infty < \infty$ is a finite number due to bounded feature values, i.e., it is the maximum difference of values across all feature dimensions. Therefore, as per Lemma A3 there exists compact domain Θ'_{θ_∞} around θ_∞ with more than one element for which $\|\nabla_r \mathcal{L}(M, H', \mathcal{A}_\theta(M, H'))\| < \frac{\epsilon_\infty}{4}$ given that $(M, H') \in \mathcal{M}_{\epsilon_{prec}}$. From this, we obtain that, for any $\theta \in \Theta_{\theta_\infty}$ in a new connected subset $\Theta_{\theta_\infty} \subseteq \Theta_{\theta_\infty} \cap \{\theta : \|\theta - \theta_\infty\|_\infty \leq \frac{\epsilon_\infty}{4}\}$ (this new set still has more than two elements and is compact and connected as an intersection of compact and connected sets),

$$
\begin{aligned}
&\|\nabla_r \mathcal{L}(M, H, \mathcal{A}_\theta(M, H))\| \\
&\leq \|\nabla_r \mathcal{L}(M, H, \mathcal{A}_\theta(M, H'))\| + \|\nabla_r \mathcal{L}(M, H, \mathcal{A}_\theta(M, H)) - \nabla_r \mathcal{L}(M, H, \mathcal{A}_\theta(M, H'))\| \\
&= \|\nabla_r \mathcal{L}(M, H, \mathcal{A}_\theta(M, H'))\| + \|errdiff(\theta)\| \\
&\leq \|\nabla_r \mathcal{L}(M, H, \mathcal{A}_\theta(M, H'))\| + \|errdiff(\theta_\infty)\| + c_{ge}\|\theta - \theta_\infty\|_\infty \\
&\leq \|\nabla_r \mathcal{L}(M, H', \mathcal{A}_\theta(M, H'))\| + \|apprfeats(H) - appfeats(H')\| \\
&\quad + \|errdiff(\theta_\infty)\| + c_{ge}\|\theta - \theta_\infty\|_\infty \\
&\leq \|\nabla_r \mathcal{L}(M, H', \mathcal{A}_\theta(M, H'))\| + c_{fe}\|H - H'\| + \|errdiff(\theta_\infty)\| + c_{ge}\|\theta - \theta_\infty\|_\infty \\
&\leq \tfrac{\epsilon_\infty}{4} + c_{fe}e_{prec} + c_{\mathcal{L}}c(\theta)\epsilon_{prec}\frac{\sqrt{|\mathcal{V}|}}{2} + \tfrac{\epsilon_\infty}{4} = \epsilon_\infty
\end{aligned}
$$

where the last equality holds for the choice $\epsilon_{prec} = \frac{\epsilon_\infty}{2c_{fe} + c_{\mathcal{L}} \sup_{\theta \in \Theta_{\theta_\infty}} c(\theta)\sqrt{|\mathcal{V}|}}$. As a final remark, $c(\theta)$ is c_c-Lipschitz almost everywhere, given that it is composed of a finite number of almost-everywhere Lipschitz derivatives. Therefore, there exists a subset of Θ_{θ_∞} that is dense on the latter, which is c_c-Lipschitz. Thus, our choice for ϵ_{prec} exists and is finite, because the denominator is positive and $\sup_{\theta \in \Theta_{\theta_\infty}} c(\theta) \leq c(\theta_\infty) + c_c\|\theta - \theta_\infty\|_\infty$ is finite, which in turn holds true given that Θ_{θ_∞} is compact and the L2 norm continuous. □

Appendix C. Algorithmic Complexity

Let us annotate the embedding dimension $K = col(H)$ and entertain a scenario with no parallelization. The generation time of embedding matrix Dim is proportional to its number of elements, and therefore, $O\big(|\mathcal{V}|K\log_2 K\big)$. Linear node feature transformations also require $O\big(|\mathcal{V}|col(X)K\big)$ time and the output linear layer requires time $O\big(|\mathcal{V}|col(H^{(L)})col(Y)\big)$. Inside ULA1D, for sparse matrix–vector multiplication on each filter parameter, we require time

$$O\big(L\,|\mathcal{E}|\,K\,col(H^{(0)})\big) = O\big(L|\mathcal{E}|K(2+\log_2 K)\big) = O(L\,|\mathcal{E}|\,K\log K)$$

assuming that self-loops are added, so that $|\mathcal{E}| \geq |\mathcal{V}|$, where L is the number of the employed filter's parameters and $|\mathcal{E}|$ is the number of nodes of the base graph, i.e., the number of non-zero elements of the adjacency metric M and not of M_{repeat}. This is because we perform a premature re-wrapping of $H^{(L)}$ into vector form (this is just a computational rearrangement) before passing it through the filter $F(\hat{M})$, effectively going back to left-multiplying each feature dimension with the normalized adjacency matrix.

However, MLP layers within ULA1D multiply the combined graph attributes $H|Dim$ with dense transformations with $(2 + ceil(\log_2 K)) \times (4 + ceil(\log_2 K))$ parameter dimensions, and the outcome of the latter with dense transformation of $(4 + ceil(\log_2 K)) \times 1$ dimensions (since $H^{(L)}$ is a column matrix). This requires total time $O(|\mathcal{V}|K\log_2^2 K)$. In the end, summing all these running times, we obtain the following time needed to run one forward pass:

$$time \in O\big(|\mathcal{E}|LK\log K + |\mathcal{V}|K(\log^2 K + col(X) + col(Y))\big)$$

In terms of memory complexity, for graph filter propagation we iteratively compute matrices $\hat{M}^n H^{(0)}$ for all $n = 1, 2, \ldots, N$ by left-multiplying the outcome for $n-1$ with $\hat{M}$ and aggregate them into one matrix with the same dimensions as $H^{(0)}$. This requires memory $O(|\mathcal{V}|\,col(H^{(0)}))$ that is independent of N, and becomes $O(|\mathcal{V}|\,K\log K)$ given that ULA1G parses $|\mathcal{V}|K$ nodes with $O(\log K)$ dimensions each. Additionally, we need to store adjacency matrices in $O(|\mathcal{E}|)$ memory, and layer parameters that similarly to before consume at worst $O(\log^2 K)$ memory for ULA1D. Input and output linear transformations

consume $O(col(X)K)$ and $O(Kcol(Y))$ memory, respectively. Overall, summing these requirements we have the following memory needs:

$$\begin{aligned} memory &\in O(\log^2 K + K(col(X) + col(Y) + |\mathcal{V}|K \log K)) \\ &= O(|\mathcal{V}|K \log K + K(col(X) + col(Y))) \end{aligned}$$

Appendix D. ULA as an MPNN

Here, we explain that any trained ULA architecture can be written as an MPNN. To begin with, both MLPs and propagation of node representation matrices one hop away constitute message-passing layers. For example, predict-then-propagate architectures like APPNP are also MPNNs. At the same time, passing the unwrapped H through an MLP is equivalent to passing through a different MLP' the wrapped version holding the same values:

$$H_{wrapped} = \left(h_1 \mathbf{1}Embed(1) | h_2 | \mathbf{1}Embed(2) | \ldots | h_{cols(H)}) | \mathbf{1}Embed(K)\right)$$

for corresponding layer representations $H^{(\ell)}_{wrapped}$ with MPNN layers:

$$\phi^{(\ell)}\left(H^{(\ell)}W^{(\ell)} + b^{(\ell)}\right) = \phi^{(\ell)}\left(H^{(\ell)}_{wrapped}W^{(\ell)}_{repeat} + b^{(\ell)}_{repeat}\right)$$

where $W^{(\ell)}_{repeat} = W^{(\ell)}|W^{(\ell)}|\ldots$ and $b^{(\ell)}_{repeat} = b^{(\ell)}|b^{(\ell)}|\ldots$. In this variation, the rewrapped version of $H^{(L)}$ is equal to $H^{(L)}_{wrapped}$.

References

1. Loukas, A. What graph neural networks cannot learn: Depth vs width. *arXiv* **2019**, arXiv:1907.03199.
2. Nguyen, Q.; Mukkamala, M.C.; Hein, M. On the loss landscape of a class of deep neural networks with no bad local valleys. *arXiv* **2018**, arXiv:1809.10749.
3. Sun, R.Y. Optimization for deep learning: An overview. *J. Oper. Res. Soc. China* **2020**, *8*, 249–294. [CrossRef]
4. Bae, K.; Ryu, H.; Shin, H. Does Adam optimizer keep close to the optimal point? *arXiv* **2019**, arXiv:1911.00289.
5. Ortega, A.; Frossard, P.; Kovačević, J.; Moura, J.M.; Vandergheynst, P. Graph signal processing: Overview, challenges, and applications. *Proc. IEEE* **2018**, *106*, 808–828. [CrossRef]
6. Page, L.; Brin, S.; Motwani, R.; Winograd, T. The Pagerank Citation Ranking: Bringing Order to the Web . 1999. Available online: https://www.semanticscholar.org/paper/The-PageRank-Citation-Ranking-%3A-Bringing-Order-to-Page-Brin/eb82d3035849cd23578096462ba419b53198a556 (accessed on 1 April 2024).
7. Chung, F. The heat kernel as the pagerank of a graph. *Proc. Natl. Acad. Sci. USA* **2007**, *104*, 19735–19740. [CrossRef]
8. Gasteiger, J.; Bojchevski, A.; Günnemann, S. Predict then propagate: Graph neural networks meet personalized pagerank. *arXiv* **2018**, arXiv:1810.05997.
9. Agarap, A.F. Deep learning using rectified linear units (relu). *arXiv* **2018**, arXiv:1803.08375.
10. Gilmer, J.; Schoenholz, S.S.; Riley, P.F.; Vinyals, O.; Dahl, G.E. Neural message passing for quantum chemistry. In Proceedings of the International Conference on Machine Learning, PMLR, Sydney, Australia, 6–11 August 2017; pp. 1263–1272.
11. Balcilar, M.; Héroux, P.; Gauzere, B.; Vasseur, P.; Adam, S.; Honeine, P. Breaking the limits of message passing graph neural networks. In Proceedings of the International Conference on Machine Learning, PMLR, Virtual, 18–24 July 2021; pp. 599–608.
12. Kipf, T.N.; Welling, M. Semi-supervised classification with graph convolutional networks. *arXiv* **2016**, arXiv:1609.02907.
13. Velickovic, P.; Cucurull, G.; Casanova, A.; Romero, A.; Lio, P.; Bengio, Y. Graph attention networks. *Stat* **2017**, *1050*, 10-48550.
14. Cai, J.Y.; Fürer, M.; Immerman, N. An optimal lower bound on the number of variables for graph identification. *Combinatorica* **1992**, *12*, 389–410. [CrossRef]
15. Maron, H.; Ben-Hamu, H.; Serviansky, H.; Lipman, Y. Provably powerful graph networks. *Adv. Neural Inf. Process. Syst.* **2019**, *32*, 2153–2164.
16. Morris, C.; Ritzert, M.; Fey, M.; Hamilton, W.L.; Lenssen, J.E.; Rattan, G.; Grohe, M. Weisfeiler and leman go neural: Higher-order graph neural networks. In Proceedings of the AAAI Conference on Artificial Intelligence, Honolulu, HI, USA, 27 January 2019–1 February 2019; Volume 33, pp. 4602–4609.
17. Zaheer, M.; Kottur, S.; Ravanbakhsh, S.; Poczos, B.; Salakhutdinov, R.R.; Smola, A.J. Deep sets. *Adv. Neural Inf. Process. Syst.* **2017**, *30* , 3391–3401.
18. Keriven, N.; Peyré, G. Universal invariant and equivariant graph neural networks. *Adv. Neural Inf. Process. Syst.* **2019**, *32*, 7092–7101.

19. Maron, H.; Fetaya, E.; Segol, N.; Lipman, Y. On the universality of invariant networks. In Proceedings of the International Conference on Machine Learning, PMLR, Long Beach, CA, USA, 9–15 June 2019; pp. 4363–4371.
20. Xu, K.; Hu, W.; Leskovec, J.; Jegelka, S. How powerful are graph neural networks? *arXiv* **2018**, arXiv:1810.00826.
21. Wang, H.; Yin, H.; Zhang, M.; Li, P. Equivariant and stable positional encoding for more powerful graph neural networks. *arXiv* **2022**, arXiv:2203.00199.
22. Keriven, N.; Vaiter, S. What functions can Graph Neural Networks compute on random graphs? The role of Positional Encoding. *Adv. Neural Inf. Process. Syst.* **2024**, *36* , 11823–11849.
23. Sato, R.; Yamada, M.; Kashima, H. Random features strengthen graph neural networks. In Proceedings of the 2021 SIAM International Conference on Data Mining (SDM), SIAM, Virtual, 29 April–1 May 2021; pp. 333–341.
24. Abboud, R.; Ceylan, I.I.; Grohe, M.; Lukasiewicz, T. The surprising power of graph neural networks with random node initialization. *arXiv* **2020**, arXiv:2010.01179.
25. Krasanakis, E.; Papadopoulos, S.; Kompatsiaris, I. Applying fairness constraints on graph node ranks under personalization bias. In *Complex Networks & Their Applications IX: Volume 2, Proceedings of the Ninth International Conference on Complex Networks and Their Applications Complex Networks, Madrid, Spain, 1–3 December 2020*; Springer: Berlin/Heidelberg, Germany, 2021; pp. 610–622.
26. Kidger, P.; Lyons, T. Universal approximation with deep narrow networks. In Proceedings of the Conference on Learning Theory, PMLR, Graz, Austria, 9–12 July 2020; pp. 2306–2327.
27. Hoang, N.; Maehara, T.; Murata, T. Revisiting graph neural networks: Graph filtering perspective. In Proceedings of the 2020 25th International Conference on Pattern Recognition (ICPR), Milan, Italy, 10–15 January 2021; IEEE: Piscataway, NJ, USA, 2021; pp. 8376–8383.
28. Huang, Q.; He, H.; Singh, A.; Lim, S.N.; Benson, A.R. Combining Label Propagation and Simple Models Out-performs Graph Neural Networks. *arXiv* **2020**, arXiv:2010.13993.
29. Zhou, D.; Bousquet, O.; Lal, T.; Weston, J.; Schölkopf, B. Learning with local and global consistency. *Adv. Neural Inf. Process. Syst.* **2003**, *16* , 321–328.
30. Fey, M.; Lenssen, J.E. Fast graph representation learning with PyTorch Geometric. *arXiv* **2019**, arXiv:1903.02428.
31. Bojchevski, A.; Günnemann, S. Deep gaussian embedding of graphs: Unsupervised inductive learning via ranking. *arXiv* **2017**, arXiv:1707.03815.
32. Sen, P.; Namata, G.; Bilgic, M.; Getoor, L.; Galligher, B.; Eliassi-Rad, T. Collective classification in network data. *AI Mag.* **2008**, *29*, 93. [CrossRef]
33. Namata, G.; London, B.; Getoor, L.; Huang, B.; Edu, U. Query-driven active surveying for collective classification. In Proceedings of the Workshop on Mining and Learning with Graphs (MLG-2012), Edinburgh, UK, 1 July 2012; Volume 8, p. 1.
34. Chen, M.; Wei, Z.; Huang, Z.; Ding, B.; Li, Y. Simple and deep graph convolutional networks. In Proceedings of the International Conference on Machine Learning, PMLR, Virtual, 13–18 July 2020; pp. 1725–1735.
35. Dunn, O.J. Multiple comparisons among means. *J. Am. Stat. Assoc.* **1961**, *56*, 52–64. [CrossRef]
36. Demšar, J. Statistical comparisons of classifiers over multiple data sets. *J. Mach. Learn. Res.* **2006**, *7*, 1–30.
37. Hollander, M.; Wolfe, D.A.; Chicken, E. *Nonparametric Statistical Methods*; John Wiley & Sons: Hoboken, NJ, USA, 2013.
38. He, K.; Zhang, X.; Ren, S.; Sun, J. Delving deep into rectifiers: Surpassing human-level performance on imagenet classification. In Proceedings of the IEEE International Conference on Computer Vision, Santiago, Chile, 7–13 December 2015; pp. 1026–1034.
39. Nunes, M.; Fraga, P.M.; Pappa, G.L. Fitness landscape analysis of graph neural network architecture search spaces. In Proceedings of the Genetic and Evolutionary Computation Conference, Lille, France, 10–14 July 2021; pp. 876–884.